RESEARCH OUTPUTS / RÉSULTATS DE RECHERCHE

Human indoleamine-2,3-dioxygenase 2 cofactor lability and low substrate affinity explained by homology modeling, molecular dynamics and molecular docking

Mirgaux, Manon; Leherte, Laurence; Wouters, Johan

Link to publication

Human indoleamine-2,3-dioxygenase 2 cofactor lability and low substrate affinity explained by homology modeling, Molecular Dynamics and Molecular Docking

Manon Mirgaux[a], Laurence Leherte[a], Johan Wouters[a]

a Namur Institute of Structured Matter (NISM), Namur Research Institute for Life, Science (NARILIS), Department of Chemistry, Laboratoire de Chimie Biologique, Structurale (CBS), University of Namur (UNamur), 61 Rue de Bruxelles, 5000, Namur, Belgium

Correspondance email: Manon Mirgaux, +32 81 72 45 69, manon.mirgaux@unamur.be

Johan Wouters, +32 81 72 45 50, johan.wouters@unamur.be

Abstract: The human indoleamine-2,3-dioxygenase 2 (hIDO2) protein is growing of interest as it is increasingly implicated in multiple diseases (cancer, autoimmune diseases, COVID-19). However, it is only poorly reported in the literature. Its mode of action remains unknown because it does not seem to catalyze the reaction for which it is attributed: the degradation of the L-Tryptophan into N-formyl-kynurenine. This contrasts with its paralog, the human indoleamine-2,3-dioxygenase 1 (hIDO1), which has been extensively studied in the literature and for which several inhibitors are already in clinical trials. Yet, the recent failure of one of the most advanced hIDO1 inhibitors, the Epacadostat, could be caused by a still unknown interaction between hIDO1 and hIDO2. In order to better understand the mechanism of hIDO2, and in the absence of experimental structural data, a computational study mixing homology modeling, Molecular Dynamics, and molecular docking was conducted. The present article highlights an exacerbated lability of the cofactor as well as an inadequate positioning of the substrate in the active site of hIDO2, which might bring part of an answer to its lack of activity.

Introduction

The hemoproteins hIDO1 and hIDO2 are specifically known to be overexpressed in many diseases. (Dolvsak2021, Uyttenhove2003) This is attributed to their occurrence in the first and rate-limiting step of the kynurenine pathway, that degrades L-Tryptophan (L-Trp) into N-formylkynurenine (NFK) (**Figure 1 and Figure S1** of the Supplementary Material). It is known that hIDO1, through the formation of metabolites of the kynurenine pathway, leads to an immunosuppression phenomenon observed in multiple types of cancer. Concerning hIDO2, the scientific literature highlights its implication in cancer (Opitz2020, Löb2009, Li2021, Fatokun2013), autoimmune diseases (Merlo2021), and recently in severe cases of COVID-19 disease. (Guo2022) Unfortunately, the study in the literature of the hIDO2 protein and the knowledge derived from it is relatively poor compared to hIDO1.
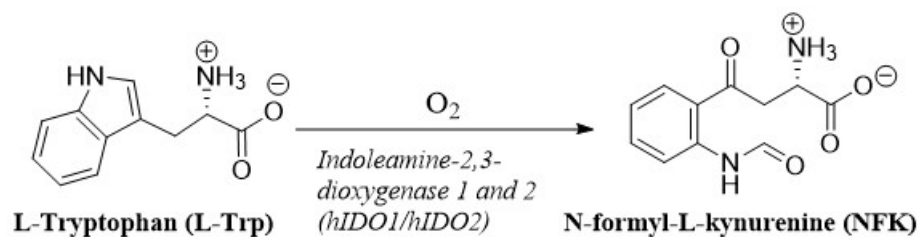
Figure 1: First, as well as rate-limiting step, in the kynurenine pathway catalyzed by hIDO1 and hIDO2.

Both proteins are paralogs: they probably come from an ancient gene duplication which occurred prior to the evolution of vertebrates. (Li2021, Mandarano2020, Ball2007, Chilosi2022, Meininger2011, Ball2009) For a long time, because of their homology (43%) (Corpet1988) and identical function, it has been assumed that hIDO2 acted in a redundant manner with hIDO1 to induce immune system escape in cancer. However, while the escape from the immune system caused by hIDO1 was due to inflammatory cascades, the involvement of hIDO2 in cancer is more complex because this pharmaceutical target is not a representative participant in the enzymatic degradation reaction of L-Trp. The hIDO2 protein has a poor affinity for L-Tryptophan, with a Km value (6.8 +/- 0.9 mM) that is not biologically relevant. (Dolvsak2021, Pantouris2014, Mondanelli2021) It is therefore not responsible for metabolite formation and immune escape in the same way as hIDO1 (hIDO1/L-Tryptophan Km value of 40μM). (Merlo2020, Mandarano2020, Löb2009) While the protein hIDO1 possess two immunoreceptor tyrosine-based

inhibitory motifs (ITIMs), the protein hIDO2 possess only the ITIM2 motif whose role is still unknown. The first ITIM motif, ITIM1, is not conserved. As a result, hIDO2 lacks signaling activity. (Fallarino2012, Mondanelli2021) Consequently, the role of this protein in cancer resistance is still under investigation. At present, hIDO1 is suspected to interact with hIDO2. (Lee2014) This could be the cause of the failure of Epacadostat, one of the most promising inhibitors of hIDO1, the latter having been unable to demonstrate an additional effect when combined with pembrolizumab during a phase 3 of clinical trial (ECHO-301) compared to pembrolizumab alone. (Long2019) However, the lack of information on hIDO2 available in the literature does not allow confirm the hypothesis.

At present, the structure of hIDO2 remains experimentally unknown. It is composed of 420 residues and it is expected to be monomeric, like hIDO1. (Dolvsak2021) The protein has two potential methionine starts (in position 1 and in position 14), but it is shown that the active form of the protein is characterized by the methionine start at position 14, with a total of 407 residues. (Meininger2011, Pantouris2014) Homology models have been already obtained on the basis of a sequence alignment of hIDO1 with hIDO2. (Meininger2011, Roehrig2016, He2021) The general fold of the protein is preserved (**Figure 2**, Upper right corner): the protein is predicted to be formed by two subunits, the larger one containing an active site composed of the heme cofactor and closed by a dynamic loop. Although the active site is conserved at 70% between hIDO1 and hIDO2 (Austin2015), Roehrig *et al.* (Roehrig2016) demonstrated that four amino acids are not conserved (Y126, C129, F164, and S167 of hIDO1 are replaced by H130, L133, I168, and T171 in hIDO2, respectively). It induces a larger (15%) binding pocket than for hIDO1 and a loss of substrate stabilization with F164 and C129 (**Figure 2,** main picture). The role of the smaller subunit is not determined yet. These models lack dynamic vision of the system, but, to the best of our knowledge, no study by Molecular Dynamics has been published for hIDO2. However, given that hIDO1 has been shown to possess high plasticity, one would expect the same observation for hIDO2. (Mirgaux2020, Mirgaux2021, Water, Pham2021) Another reported structural information is that two polymorphs of hIDO2, namely R235W and Y346X, are present in more than 25% of the Caucasian population (Roehrig2016). (Li2021, Li2009) The role or reason for the appearance of these polymorphs

is still unknown. However, it can be shown that it reduces the activity of the protein even more than for the wild type protein (90% for R235W and 100% for Y346X). (Witkiewicz2009)
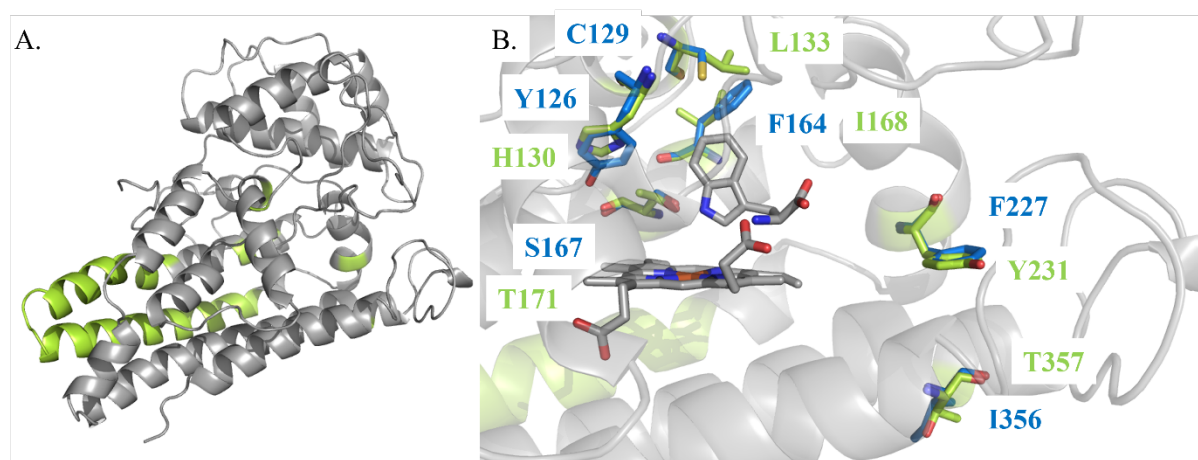

Figure 2: A. Global fold of hIDO2 and highlighting (in green) of the non-conserved parts in the sequence in comparison to hIDO1. B. Variation in the amino acids composition (hIDO1 in blue and hIDO2 in green) as observed in the homology models.

The lack of structural knowledge of hIDO2 is an obstacle to the understanding of its role in diseases and to the design of inhibitors. No data is reported in the literature on its plasticity, the behavior of the JK'-loop nor the lability of its heme cofactor. Additionally, it is difficult to understand why an enzyme with more than 40% of sequence similarity to hIDO1 does not catalyze the same reaction as does its cousin. To provide more information on this protein, the present study reports a computational analysis of the structure of hIDO2 by means of a multidisciplinary approach mixing homology modelling and Molecular Dynamics (MD) simulations. It allows, for the first time, to evaluate the effect of the presence of the cofactor in the enzyme and to rule on its potential lability. Moreover, with a complete and dynamic model of hIDO2, the docking analysis of L-Trp allows to hypothesize that the inadequate pre-organization of the substrate in hIDO2 might be a reason of its very low efficacy compared to hIDO1w. Altogether, the results provide a first complete structural analysis of hIDO2.

Material and methods

Homology modelling of hIDO2

The model of hIDO2 was obtained using the Swiss Model program (Waterhouse2018, Guex2009, Studer2020) starting from the PDB structure 7a62. (Mirgaux2020) The sequence of hIDO2 was the one described in UniProt (The Uniprot Consortium), with M14 as the first residue in order to consider the active form of the enzyme. The heme, missing from the model, was added from its position within hIDO1, with an initial distance between iron and H347 of 2.2Å.

Molecular Dynamics studies of hIDO2 in the absence of ligands

Molecular dynamics simulations of hIDO2 were performed on the basis of the structure obtained by homology. The protein was considered with (holo form) and without its heme cofactor (apo form). The two hIDO2 polymorphs reported in the literature (R231W and Y346X) were designed using Pymol (Schoedinger2015). The hydrogen atoms were added to the homology model using the GROMACS *pdb2gmx* tool. MDs were run using GROMACS 2020 (Abraham2015) with the CHARMM27 force field (MacKerell2000) and the CMAP correction for the protein. The solvation of the models was performed with all-atom TIP3P and coarse-grained SIRAH water particles according to the same methodology as reported for hIDO1. (Mirgaux2020) The total charge of the system was neutralized with sodium ions randomly placed in the bulk of the SIRAH water particles. The methodology used for system minimization, equilibration and production stages was also applied as in our previous publication. (Mirgaux2020) All models were analyzed in triplicates, with three different initial random velocity sets. The production steps lasted 300 ns, with a time step of 2 fs.

Molecular docking calculations of hIDO2

The induced-fit docking of L-Trp in the active site of hIDO2 was performed with the holo structure of hIDO2 obtained after 300 ns of the MD production stage. It was performed with the Maestro software (version 12.4) and associated modules (Madhavi2013, Greenwood2010, Shelley2007, Harder2016). First, the Protein Preparation Wizard (Madhavi2013) was used to prepare the protein of interest. A preprocessing of the structure was performed in order to assign the binding orders, to add the hydrogens

to the structure, and to build the disulfide bridges (Greenwood2010, Shelley2007). This step also allowed to define the redox state of the heme cofactor. After optimization of the hydrogen bonds contained in the protein, a general minimization was performed using the OPLS3e force field. (Harder2016) The ligand was prepared using the LigPrep module with the same force field allowing conversion of the 2D structure to 3D as well as addition hydrogen atoms. Bond length and angle values were corrected by structure minimization. The different ionization sates were generated by Epik. (Greenwood2010, Shelley2007, Harder2016) The docking was then carried out with the with Glide software by the Induced fit docking method, considering the OPLS3e force field. (Harder2016) The iron atom of the heme cofactor present in the active site of the protein served as the center for the box defining the volume. The size of the box was defined as less than or equal to 20Å. The ligand was docked in a flexible way, by evaluating the different possible conformations within 2.5 kcal/mol of the minimum. The induced-fit module performs a so-called Glide pre-docking of the ligand and generates 20 poses. After application of an automated side chain trimming, based on B-factors and applied with a van der Waals scale of the receptor and ligand of 0.70 to 0.50 respectively, optimization of the side chains located within 5Å of the ligand is performed. These induced-fit corrected poses were redocked into the structures within 30.0 kcal/mol of the best structure (in standard-mode precision (SP)). The results showed the 20 best ligand positions according to the Glide score. A negative GlideScore indicates a more favorable binding. The poses with the best Glide score and the closest pose to the known reactive position of hIDO1 were kept in order to perform MM-GBSA analyses as well as a further investigation by Molecular Dynamics.

MM-GBSA evaluations

In order to evaluate the affinity of L-Trp, MM-GBSA calculations were performed using the Maestro Prime MM-GBSA modules. (Jacobson2002, Jacobson2004) They were run using the VSGB solvatation model (Li2011) with the OPLS3e force field. The enzyme was kept rigid to preserve a conformation close to the docked conformation.

Molecular Dynamics studies of hIDO2 in presence of L-Trp

As none of the docking orientations is equivalent to the reactive position observed in hIDO1 (PDB code: 7nge), MD simulations of L-Trp in the active site of hIDO2 were performed from the docking poses characterized by the best Glide score pose (pos1) and the pose closest to a pre-reactive position observed in comparison to hIDO1 (pos6). The ligand topology files were created using the SwissParam software. (Zoete2011) The methodology followed is exactly the same as in the case of ligand-based simulations of hIDO1 (Mirgaux2021) for model building, minimization, equilibration, and production. The ligands are free to move during the whole simulation.

Results

Design of a homology model

As detailed previously, the hIDO2 structure was obtained through homology modelling with hIDO1 as the template. The helices of its large subunit are named following the alphabetical order, from A' to K', in reference to the loops in hIDO1. Due to differences into the sequence of hIDO2 and hIDO1, model discrepancies between hIDO2 and hIDO1 are observed at three places along the protein sequence, at the level of the N-terminal part (M1 to L16 of hIDO2, not present in hIDO1), the EF'-loop (R284 to E288 of hIDO2, shorter than in hIDO1), and the JK'-loop (A360 to G383 of hIDO2, longer than in hIDO1) (**Supplementary Material, Figure S2**). The resulting homology model begins at residue 17 of the protein due to the lack of information about the N-terminal fragment. The heme cofactor was added in the homology model of hIDO2 by aligning the structure of hIDO2 with the one of hIDO1 (monomer C of 7a62, rmsd of 0.09Å). The alignment of the homology model with the structure retrieved from the AlfaFold server (Jumper2021, Varadi2022) presents a rmsd of 1.0Å, i.e, the same imprecision as the homology model (the N-terminal part of the protein, the JK'-loop, and in the DE'-fragment).

Study of the hIDO2 structure with the heme cofactor

MD simulations were performed starting from the hIDO2 homology model. Since experimental results suggests that the cofactor is labile in hIDO2 (Mirgaux2022), the covalent link between H347 and the cofactor is not explicitly fixed. The three replicates converge towards the same folding (r.m.s.d. value of 2.5Å +/- 0.1Å). The parts that diverge among the replicates (**Supplementary Material, Figure S3)**

are also those that diverge from the model obtained by homology (r.m.s.d. value of 2.5Å +/- 0.5Å), due to the great flexibility of these fragments. The main differences are located in the helix F', the heme binding site, the DE'-fragment, and the JK'-loop.

In the hIDO2 homology model, the fold of the helix F' is biased by the structure of hIDO1. Its length is also reduced due to the GGHA gap occurring after K287 and E288 in the hIDO2 sequence. During the MD equilibration and production stages, the helix F' reorganizes and initiate the formation of a helix turn ahead in the sequence (**Figure 3, A.**). This loop is likely to be rather flexible since its conformation slightly varies between the MD replicates. As observed for the F' helix, the heme binding site is also an area of divergence between the homology model and the MD structures. The folding of the heme binding site demonstrates a change in the position of the cofactor in its pocket in comparison with the homology model (in orange, **Figure 3, B.**). This reorganization occurs very quickly during the equilibration steps of the simulation. It can be explained by a rearrangement of the amino acids of the I' helix (G325 to T352). Notably, the H347 that coordinates the heme cofactor reorients and loses its stabilizing role (**Figure 3**, **B.**). As a result, during the production phase, the cofactor is not coordinated to the protein and is much more mobile. This non-coordination is observable in all replicates. A mutagenesis study, based on the sequence alignment of hIDO2 and hIDO1, highlights that this lack of H347-heme coordination is not due to any major change in the sequence of hIDO2 (**Supplementary Material, complementary experiments**). Despite this rearrangement, the heme is stable in its new position during the production phase, as shown by a r.m.s.d. profile calculated versus the initial position (**Figure 3**, **C.**). The G265-Q270 fragment defining the pocket A of the active site is also impacted by the reorganization, and its conformation varies in comparison from the homology model (**Figure 3, D**.). More precisely, the fragment G265-Q270 adopts two possible conformations during the simulations, with S267 oriented toward the heme cofactor and A268 varying in position.
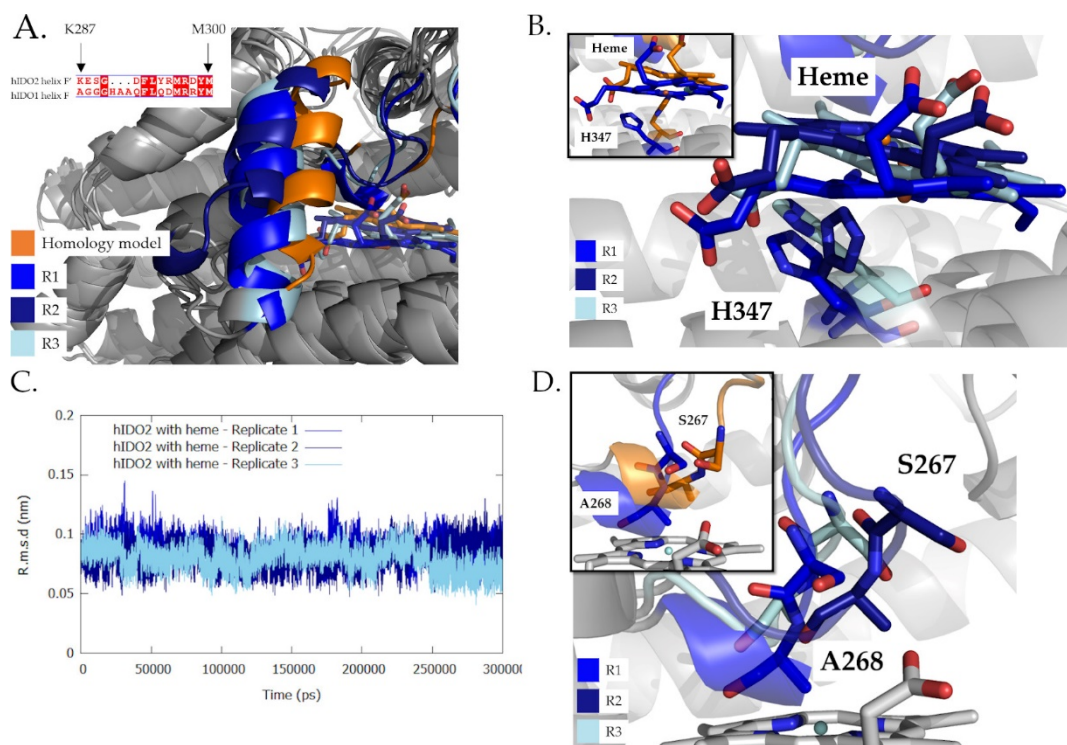
Figure 3: Comparison of the homology model (in orange) and the MD replicates after 300 ns at 310 K and 1 bar (in different shades of blue: R1 = medium blue, R2 = dark blue and R3 = light blue). A. Structural differences (highlighted in colors) between the replicates and the homology model for the helix F' and the heme binding site.   B. Positions adopted by the heme and the H347 fragment in the MD replicates (main figure) and the homology-based model (up corner).   C. R.m.s.d profile of the heme group during the simulation in comparison to the starting position. D. Positions adopted by the G265-Q270 fragment in the MD replicates (main figure) and the homology-based model (up corner).

The flexibility of the JK'-loop is also highlighted. After relaxation, the loop is observed between residues A358 and R380. It contains a large number of proline, alanine, and lysine residues (four of each type (occurrence: 18%)). Due to such large amounts, an alternation of polar and apolar parts is observed (**Figure 4, A**.). The loop can be separated into two parts, an N-terminal part from A358 to P374 and a C-terminal part from Q375 to R380. The N-terminal part is itself subdivided into two parts, i.e., N1 from 358 to 368 and N2 from 369 to 374. The N1 part is polar and, in some MD frames, it adopts an alpha helix fold between residues K366 and N368, that increases the fluctuation of the residues as illustrated in the R1 MD replicate. The N2 part is mainly apolar, and is more agitated than N1 and the C-terminal part. The flexibility of the C-terminal part is much lower than the one of the N2 part, but larger than the

N1 part. The mean fluctuation of the JK'-loop is 0.30nm +/- 0.01nm, i.e., a threefold increase in comparison to the mean total fluctuation of the protein (**Figure 4**, **B.** and **C.**). The classification of the JK'-loop conformation is based on the distance between A268 (central residue in the active site) and R380 (residues from the C-terminal part of the loop), in the same way as the classification for the JK-loop in hIDO1 is done (where A268 is the homologous of A264 and R380 is homologous of K377) (Mirgaux2020, Mirgaux2021). Trajectories are classified according the distance between A268 (Cb atom) and R380 (N1 atom): closed (distance < 10 Å), intermediate (10 Å < distance < 16 Å) and open (> 16 Å). It is shown that the stabilization of the C-terminal part depends on the conformation adopted by the loop. This part of the JK'-loop is characterized by a high flexibility, with a slight advantage for the open and intermediate conformations (**Figure 5**). The number of H-bonds within the DE'-fragment (defined from V227 to G250) varies only slightly between the replicates (R1 = 1.8, R2 = 2.2, R3 = 2.2). It highlights that the DE'-loop can adapt its conformation to the change in the JK'-loop position so as to avoid gaps between the JK'- and DE'-loops on the enzyme surface. Taken together, the enhanced flexibility of the protein, the unfolding of the F' helix, the lack of interaction between H347 and the cofactor and the open loop are elements that decrease the constraint of the cofactor in the active site and increase the likeliness of lability. In all cases, the heme does not leave the protein but moves inside the active site.

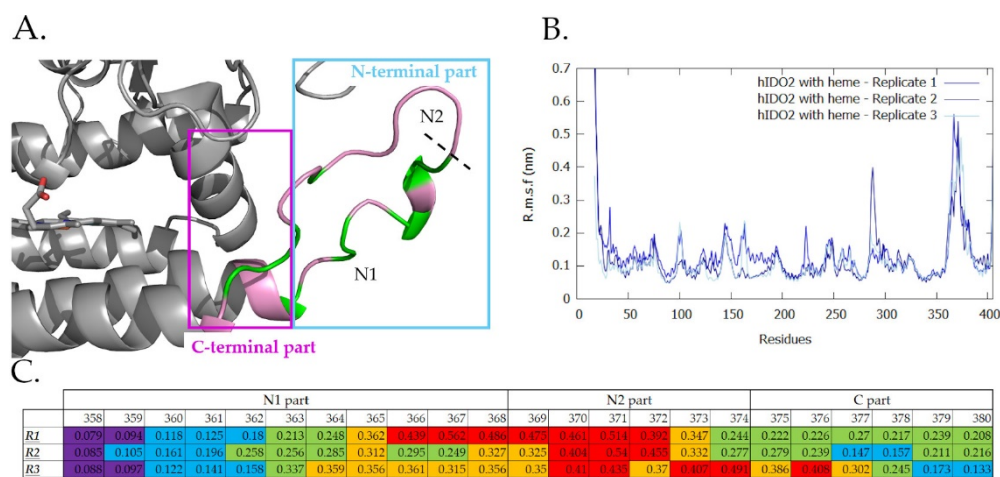|	N1 part											N2 part						C part					
	358	359	360	361	362	363	364	365	366	367	368	369	370	371	372	373	374	375	376	377	378	379	380
R1	0.079	0.094	0.118	0.125	0.18	0.213	0.248	0.362	0.439	0.562	0.486	0.475	0.461	0.514	0.392	0.347	0.244	0.222	0.226	0.27	0.217	0.239	0.208
R2	0.085	0.105	0.161	0.196	0.258	0.256	0.285	0.312	0.295	0.249	0.327	0.325	0.404	0.54	0.455	0.332	0.277	0.279	0.239	0.147	0.157	0.211	0.216
R3	0.088	0.097	0.122	0.141	0.158	0.337	0.359	0.356	0.361	0.315	0.356	0.35	0.41	0.435	0.37	0.407	0.491	0.386	0.408	0.302	0.245	0.173	0.133

Figure 4: Characterization of the structure obtained after 300 ns MD simulation at 310 K and 1 bar for holo hIDO2. A. Conformation of the JK-loop. Proportion of polar residues (green) and apolar residues

(pink) around the N-terminal and the C-terminal part. B. R.m.s.f. profiles for the three replicates. C.

Mapping of r.m.s.f. values for residues of the JK'-loop. Warm colors reflect larger fluctuations.

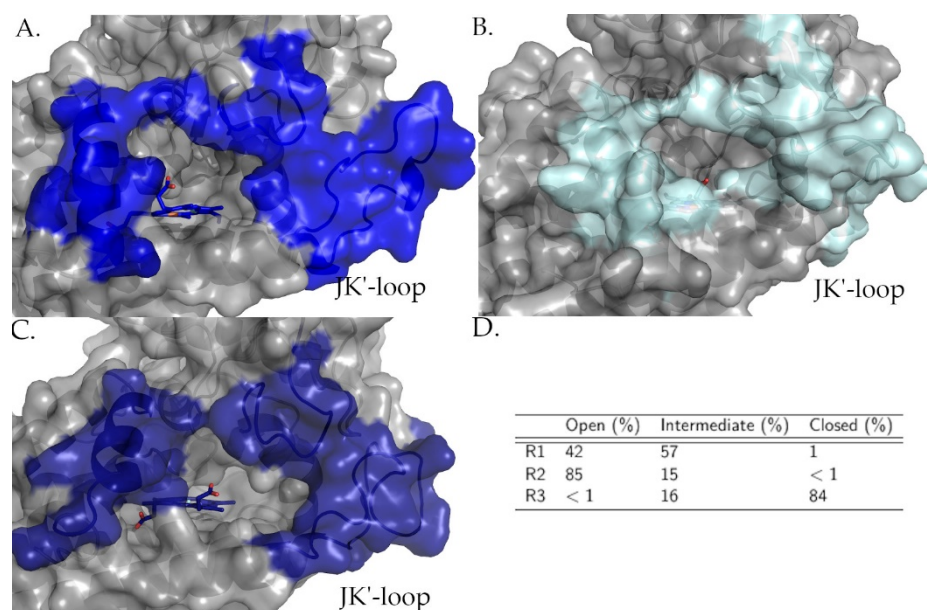|	Open (%)	Intermediate (%)	Closed (%)
R1	42	57	1
R2	85	15	< 1
R3	< 1	16	84

Figure 5: Characterization of the structure obtained after 300 ns MD simulations at 310 K and 1 bar for the JK'-loop in holo hIDO2. van der Waals surfaces around the heme cofactor and conformations adopted by the JK'-loop in MD replicates (A. R1, B. R2, C. R3). D. Percentage of open, intermediate and closed conformations in the MD replicates.

Comparison of the holo and the apo form of hIDO2

As the cofactor of hIDO2 is free to move in the active site, the MD study of the plasticity of the apo form of hIDO2 was performed in triplicates. The three simulations showed a convergence towards the same folding during the production stage, and the r.m.s.f. profiles as well as the r.m.s.d. profiles are similar (**Supplementary Material, Figure S4**, A. and B.). From a quantitative point of view, the structure changes observed along the MD trajectories highlight that the main differences occur at the level of the fragment G265-Q270, the helix F', as well as the helix I' (**Supplementary Material, Figure S4**, C., D., and E.). Such differences can be explained by an exacerbated plasticity of these parts without marked increase of the flexibility. This is due to the absence of the cofactor in the active site which, when present, has a restrain effect on the protein architecture. For example, the G265-Q270 fragment adopts multiple conformations within the replicates along the trajectories. Since these conformations

were stable for the holo form, the absence of heme allows an easier transition between the conformations. In view of the consistency between the replicates, the results are reported for the replicate R1 only.

The comparison of the final snapshot of the apo and holo forms highlights that the absence of the cofactor causes large-scale changes in the relative positioning of the G265-Q270 fragment and the F', G', K' helices of the protein (**Figure 6**, A.). It supports the already mentioned importance of these helices in the cofactor lability in hIDO2. Due to the movement of these different secondary structure elements, a global closure of the active site is observed, thus no longer allowing the binding of a new free heme group from the solution (**Figure 6**, B.). The conformation adopted by the C-terminal part is open, as it is in the presence of cofactor. The van der Waals surface at the level of the loop is almost identical, with and without cofactor (**Figure 6**, B.). The loop motion is anti-correlated to the G265-Q270 fragment and to the F', G', K' helices of the protein (**Figure 6**, C.). It can be concluded that in the case of the hIDO2 apo form, the heme binding site is closed by the change of conformation of the F', G', and K' helices, but not by the JK'-loop. The JK'-loop is only slightly impacted by the absence of the cofactor in terms of r.m.s.f. values and conformation (**Figure 6**, D.).
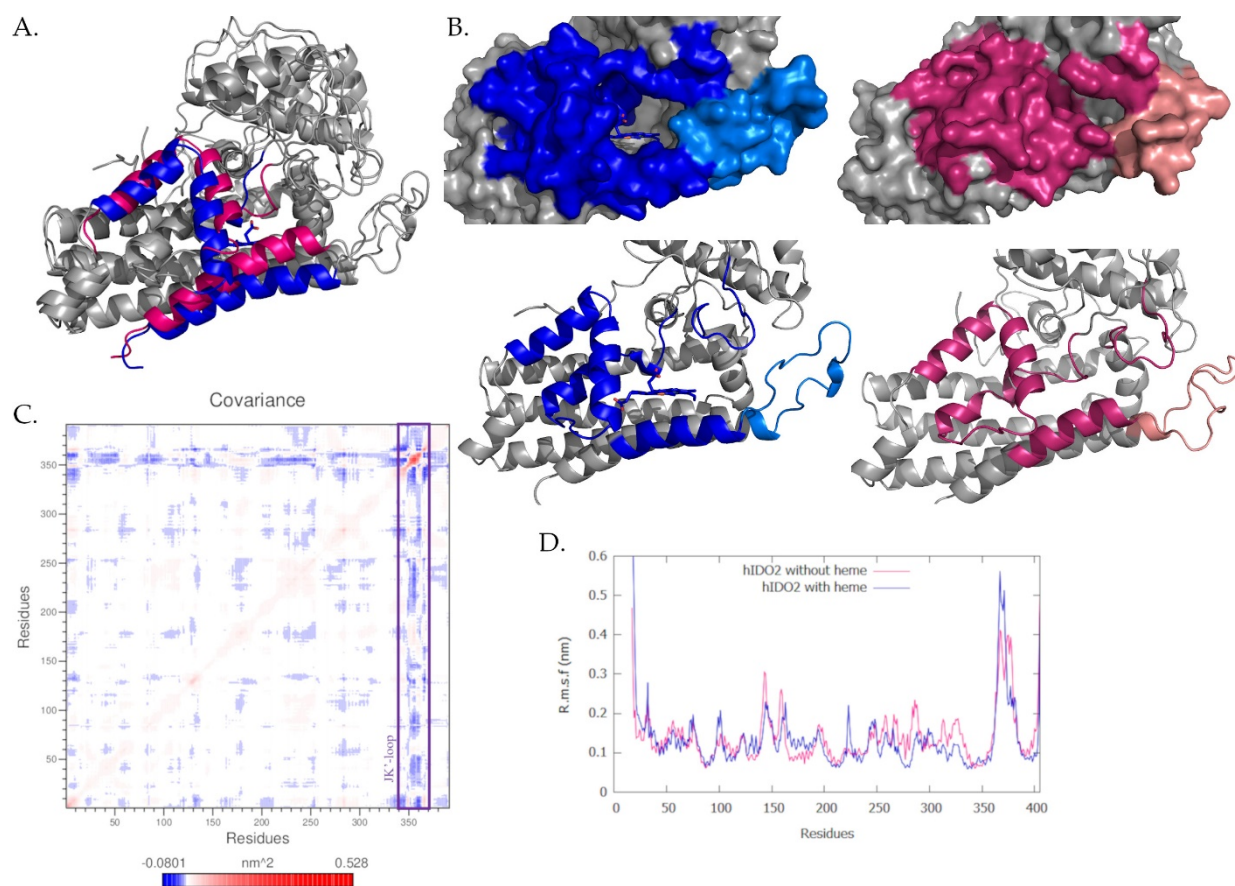
Figure 6: Characterization of the apo hIDO2 structure obtained after a 300 ns MD simulation at 310 K and 1 bar (in magenta) and comparison with the structure with the cofactor (in blue). Main differences between the apo and the holo proteins are highlighted in colors (JK'-loops are represented with light colors). A. Global folding of the two protein forms. B. Influence of the cofactor presence on the van der Waals surface of the proteins and corresponding secondary structure. C. Covariance map of the protein residues for R2. D. R.m.s.f. profiles of the apo and holo proteins.

Influence of the polymorphism on the heme lability

Two polymorphic forms of hIDO2 are observed among the Caucasian population. These forms are 1) a mutation of R235W 2) a deletion of a piece of sequence from Y346 to the end of the protein. The replicate MD simulations (**Supplementary Material, Figure S5**) highlight that the R235W mutation affects the secondary structure of the G265-Q270 fragment, the F' helix, and the JK'-loop (**Figure 7**, A.). The heme position is modified such as it adopts a position further in the active site, closer to the JK'-loop and to R380. Even if the JK'-loop adopts a closed conformation at the C-terminal extremity,

the deconstruction of the F' helix leads to a large opening in front of the heme (**Figure 7**, B.). The motion of the JK'-loop is decreased by the mutation while the flexibility of the F'-loop varies according to the replicates leading to different conformations (**Supplementary Material, Figure S5**). This position change of the heme comes from a rearrangement of residues in the active site (**Figure 7,** C. for R1 and **Supplementary Material, Figure S5** for R2 and R3). The neutral residue W235, which replaces the positively charged R235, is not oriented in the same way as R235. Because of this reorientation and the absence of a positive charge to repel R380, R380 is attracted towards the active site pocket. It leads to new interactions between R380 and the cofactor, W235, R295 (included in the helix F'), and the G265-Q270 fragment, and is characterized by an anti-correlated motion (**Figure 7, D.**, violet square). As a result, an induced fit of the entire heme binding pocket occurs and is associated with a contraction of its volume (**Supplementary Material, Figure S6)**. Also, since the cofactor is no longer bound to H347 in the R235W mutant, the volume contraction leads to the exit of the cofactor from active site. This change in the cofactor position impacts the conformation of the F' helix. The positively charged amino acids of the helix F' modify their position in order to compensate for the resulting stabilization of the heme. Thus, K287 and R295, which do not interact with the cofactor in the WT protein, are correlated with each other (**Figure 7, D**, red square) and establish interactions with the carboxylate groups of the cofactor and the positively charged residues, observed in some frames of the MD replicates and. It causes a loss of helix folding between K387 and D291. This pulls the heme out of the active site as observed through the MD trajectories (**Figure 7**, C.).
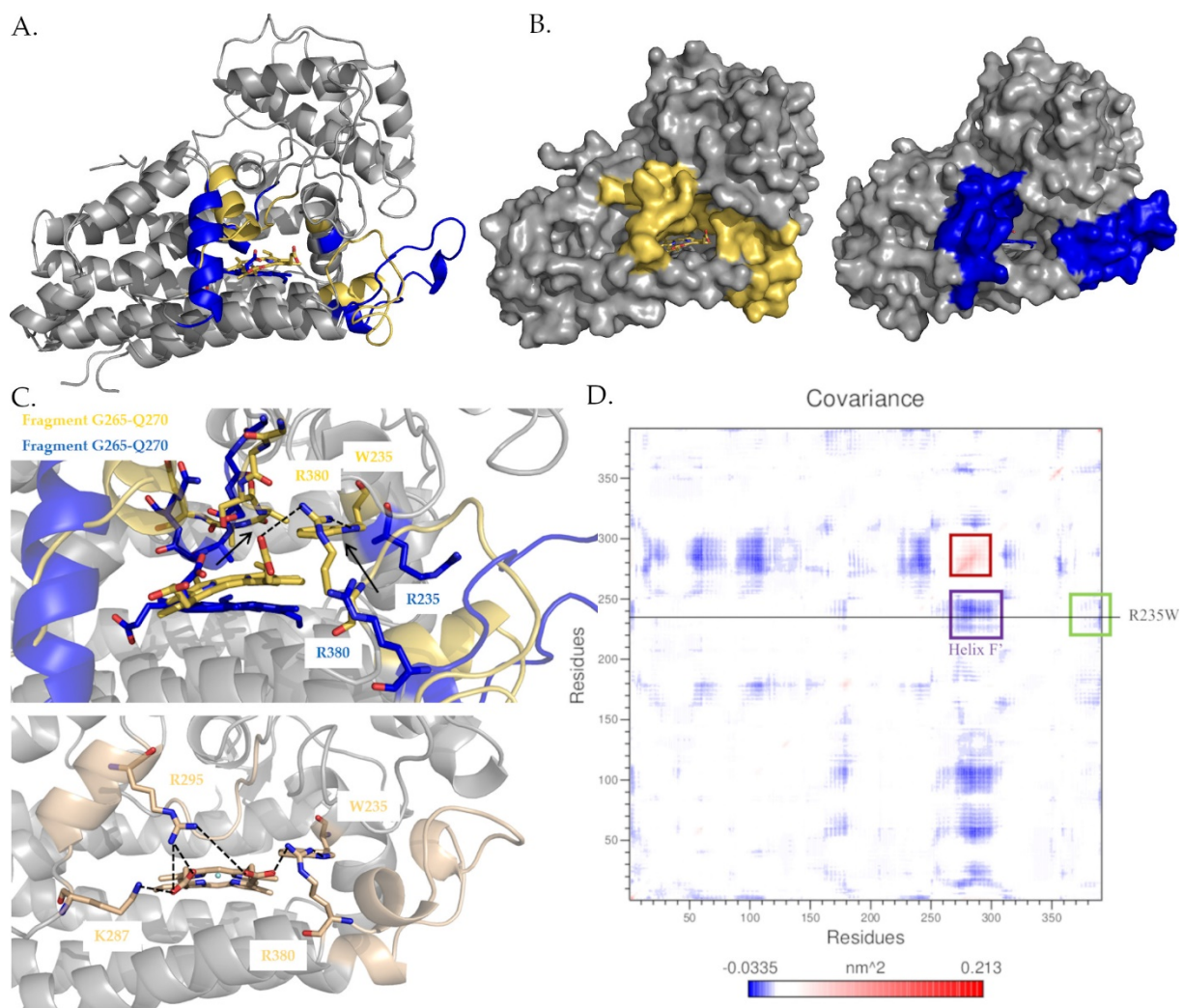
Figure 7: Characterization of the hIDO2 structure with the mutation R235W obtained after a 300 ns MD simulation at 310 K and 1 bar (R1, in yellow, R2 in wheat). A. Comparison with the structure after 300 ns for R1 with the cofactor (WT protein, in blue). Main differences between the WT protein and the R235W mutant are highlighted in blue and yellow colors respectively. B. Open surface of the mutant protein hIDO2 after 300 ns from the MD replicate R1 and contraction of the heme binding pocket. Comparison with the surface for WT protein after 300 ns (in blue). C. (Top) Induced-fit caused by the R235W mutation on the JK'-loop residues (R1). (Bottom) Conformation of K287, R295, and R380 in the trajectory at 220 ns of the MD simulation of the R235W protein, at 310 K and 1 bar (R2). D. Covariance map of the protein residues as obtained for the MD replicate R3. The green, violet, and red squares point to R380, F' helix, and residues 265-270, respectively.

Regarding the second polymorph, the deletion of residues Y346 to P405 involves a displacement of the cofactor (**Figure 8**, A.). In each MD replicate (**Supplementary Material, Figure S7)**, there is a loss in the occupancy of the heme binding pocket. Despite the fact that the replicate trajectories of the heme are not all identical, the heme tends to occupy a new pocket, formed by H222, F230, Y231, and R235. The structural differences with the WT protein are again observable at the level of the E', F', G', H', and I' helices (**Figure 8**, A. and D.) and the G265-Q270 fragment. The van der Waals surface of the protein shows an opening of the protein (**Figure 8,** B. and E.). It is thus suggested that the heme can be free to leave its binding site for another protein with a higher affinity. Electrostatic interactions with R235 and/or R344 stabilize the carboxylate moiety of the cofactor (**Figure 8**, C. and F.). A hydrophobic environment formed by the residues V174, L218, M221, F230, I234, L238, and A268 also participate to the heme stabilization, as well as the hydrogen bonds formed with Y231 and H222. From all these evidences, it is assumed that this hIDO2 polymorph strongly impacts the lability of the cofactor, mainly by causing conformational changes in the F' helix and, if present, in the JK'-loop.
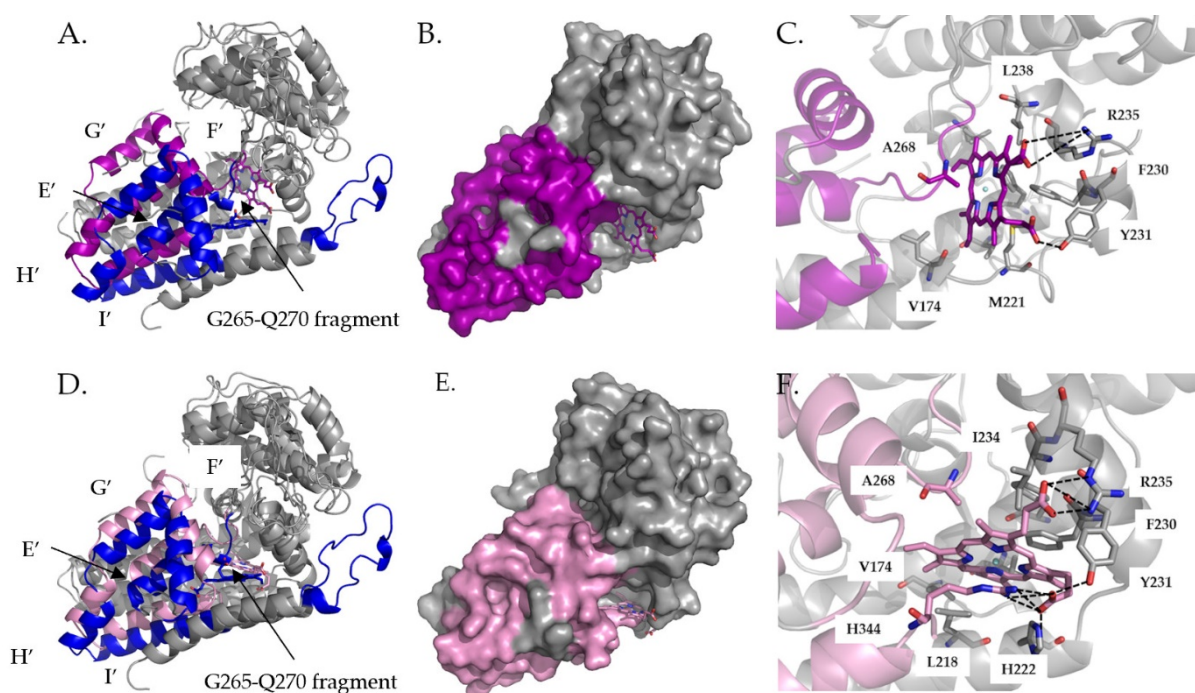

Figure 8: Characterization of the hIDO2 structure with the deletion Y346X obtained after 300 ns MD simulation at 310 K and 1 bar for (R1: in purple, R2: in pink). A. and D. Comparison with the structure containing the cofactor (WT protein, in blue). Main differences between the WT protein and the deletion

polymorph are highlighted in blue and purple/pink colors, respectively. B. and E. Open surface of the protein hIDO2 caused by the deletion. C. and F. Interactions between the heme cofactor and the protein in its new position

Docking and MD simulations with L-Trp into the active site of hIDO2

The experimental and the literature data indicate that L-Trp has a low affinity for hIDO2. To generate a structure of hIDO2 complexed to its substrate, molecular docking calculations of L-Trp were performed on the holo structure obtained by MD at the end of the 300 ns MD trajectory. The calculations were carried out using the Maestro program, through an induced fit method allowing a rearrangement of the side chains of the protein. Twenty-one docking orientations were obtained for L-Trp in hIDO2 with docking scores ranging from -6.84 kcal/mol to -4.835 kcal/mol. None of these orientations is equivalent to the pre-reactive position observed in hIDO1 (PDB code: 7nge). Nevertheless, two poses were analyzed, namely the best score pose (pos1) and the pose closest to a pre-reactive position (pos6) (**Figure 9, A. and B.**). Pos1 shows the L-Trp in a position where the indole nitrogen atom points to the main chain carbonyl of G266. The polar part of the ligand is stabilized by the heme. The orientation of R235 does not allow to stabilize the carboxylate of the substrate. The active site is open due to the relative position of the side chains S267, A268, and A269. For pos6, the orientation of the polar part of the ligand is similar to pos1 but the indole ring is flipped involving that the ring nitrogen interacts with the iron atom of the heme. The active site is closed. Consequently, few interactions are established with the ligand. These interactions mainly occur at the level of the G265-Q270 fragment. For both poses, F167, F230, L238, and L355 provide a hydrophobic environment to stabilize the aromatic part of the L-Trp and R380 interacts with the carboxylate part of the substrate. MM-GBSA calculations achieved using the Prime MM-GBSA module lead to similar binding ΔG values for both poses, namely -35.48 kcal/mol for pos1 and -34.56 kcal/mol for pos6. Since the observed complex is the Michaelis complex and not the transition state, it is difficult to draw conclusions on the activity of hIDO2. In addition, whether the dynamics of an enzymatic system influences the rate of a reaction is currently a highly debated subject, as illustrated and discussed, e.g., in (McGeagh2011, Warshel2016, Schwartz2023). However, these first results provide the basis for investigating the preorganization of the substrate within the enzyme. If L-

Trp is positioned as it is in pos1, the resulting molecular arrangement may not lead to a reaction. If it is positioned as in pos6, the coordination with iron prevents the activation of the dioxygen, mandatory to form the transition state and to allow the enzymatic reaction.

During the MD simulation of pos1, L-Trp globally remains at the same position even if the orientation of the indole moiety varies slightly (**Figure 9, C.**). Despite the slight reorientation of the indole ring, L-Trp does not move towards the pocket A due to a steric hindrance at the level of the aromatic part. In contrast to pos1, pos6 is not stable at all during the MD simulation. From the beginning of the production stage, the ligand leaves the active site of hIDO2. Then, it moves at the surface of the protein, approaching from time to time the opening of the heme pocket. The MD observations are consistent with the MM-GBSA calculations, i.e, pos1 is seen as more stable than pos6. Nevertheless, both MD simulations show a stabilization of the JK'-loop in the presence of L-Trp inside or outside the enzyme. In both cases, the loop is so stable that it hardly varies in conformation with time (**Figure 9, D.** and **Supplementary Material Figure S8** for r.m.s.f. values). The conformation adopted by the loop is intermediate at the C-terminal extremity.
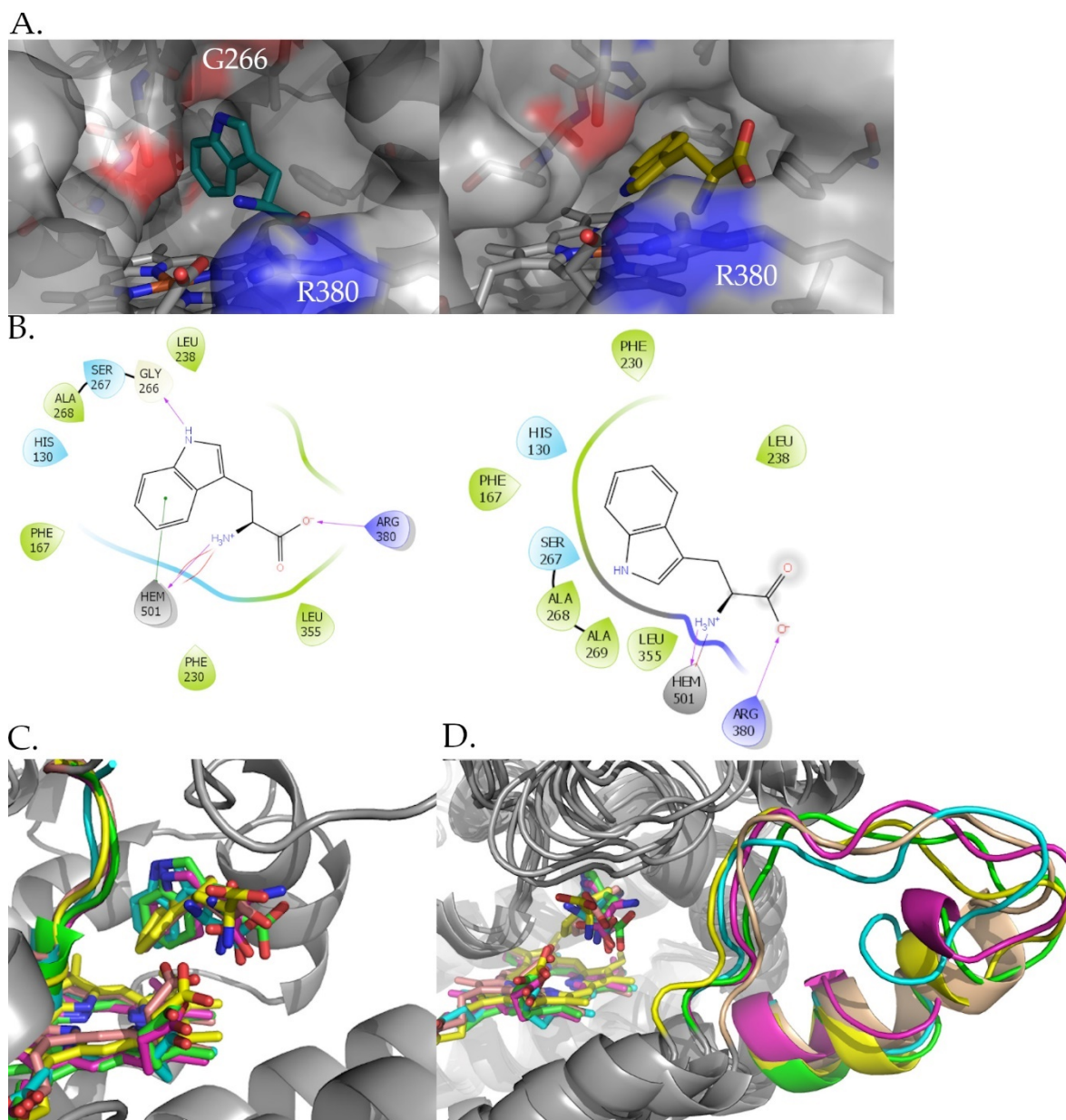
Figure 9: Investigation of L-Trp bounded form of hIDO2 by molecular docking calculations and Molecular Dynamics. A. Two analyzed poses obtained by docking of L-Trp into hIDO2. Protein is presented with the van der Waals surface of the residues in the active site for pos1 (left) and pos6 (right). B. Interactions map for two analyzed poses obtained by docking of L-Trp into hIDO2 (left: pos1, right: pos6). C. Snapshots of the 300 ns MD trajectories of the L-Trp bound to hIDO2 at 100, 150, 170, 200, and 300 ns, at 310 K and 1 bar. Pos1 is used as the starting MD ligand position. The different colors show the different snapshots from the MD. D. Conformations of the JK'-loop as obtained from the 300 ns MD trajectories of the L-Trp bound to hIDO2 at 100, 150, 170, 200 and 300 ns, at 310 K and 1 bar

with pos1 as the starting MD ligand position. The different colors show the different snapshots from the MD.

MD studies performed by our research group for hIDO1 from crystal structures allow to compare the two enzymes. (Mirgaux2021) In such X-ray diffraction experiments, L-Trp was observed in three distinct positions (**Supplementary Material**, **Figure S9**). In two of them, L-Trp occupies an intermediate position (PDB code: 7p0n and 7p0r) while the third one presents L-Trp in a pre-reactive position (PDB code: 7nge). The MD study based on these crystal structures (Mirgaux2021) showed that the JK-loop changes its conformation upon arrival of the substrate. The closing of the JK-loop allows the displacement of L-Trp in pocket A (or conversely, the displacement of the ligand allows to close the loop). In its pre-reactive and most stable position (**Figure 10**), the substrate/protein complex has a mean short-range Coulomb and Lennard-Jones energies average of −327.5 kJ/mol ± 41.4 kJ/mol (calculated from the complete 300 ns of simulation). The interactions of L-Trp with K373 and K377 are crucial for such a mechanism. Alternatively, the different conformations of the dynamic loop could be related to different magnitudes of C-terminal fluctuations, depending on the folding steps (**Figure 10,** B.). During the substrate positioning, such conformation fluctuations must be large enough to displace the ligand, and the resulting r.m.s.f. values are large in comparison to the case without substrate. In the pre-reactive position, the loop closes and remains stable. Flexibility of the C-terminal part of hIDO1 is therefore essential for the completion of the reaction. During the substrate positioning, there is a decrease in the pKa values of the two lysines K373 and K377 following the trapping of what within the protein, as calculated using PropKa Web servers (Li2005) (**Table 1**). Likewise, R231 becomes more basic. These changes in pKa are therefore related to conformational changes of the JK-loop. In hIDO2, the only stable positions are those where L-Trp is in the intermediate position, such as pos1, similar to the intermediate positions of hIDO1. Further studies revealed that it is actually not possible to stabilize the substrate in a position analogous to the pre-reaction position of hIDO1 (**Supplementary Material, Figure S10**). As a result, the substrate/protein complex has a much less negative mean interaction energy than hIDO1 with a value of −173.9 kJ/mol ± 50.7 kJ/mol (evaluated from the short-range Coulomb and Lennard-Jones energies averaged from the complete 300 ns of simulation). This is, however, more stable than L-

Trp in the analogous intermediate position, before displacement, in hIDO1 (−97.3 kJ/mol ± 46.6 kJ/mol evaluated from the short-range Coulomb and Lennard-Jones energies average of the 50 first frames of the MD simulation starting from hIDO1-intermediate structure.). The explanation put forward to justify the difference of substrate organization in the enzyme comes from the difference in plasticity of the two proteins. Indeed, the MD trajectories of hIDO2 with L-Trp in the intermediate position, show that the loop is stabilized by the presence of the substrate and retains its intermediate position (**Figure 10**, C.). Conversely, for the hIDO1 homologous position, the C-terminal end was so agitated that it outperformed the ligand-free values of the N-terminal end (**Figure 10**, B.). An hypothesis is that the loop in hIDO2, strongly stabilized by the poorly positioned L-Trp, does not allow the closing of the active site, and L-Trp is not pushed into pocket A. Such a stabilization of the JK'-loop should not lead to a decrease in pKa values due to the closure of the loop and the change of environment of the polar residues. Moreover, when placed in an intermediate position in hIDO2, L-Trp is more stable than in the analogue position in hIDO1; the hIDO2 substrate remains in its local energy minimum. That leads to the conclusion that misoriented L-Trp can be stabilized in hIDO2 even if L-Trp is not ideally placed to form a reactive transition state. It has been reported that an identical pre-organization pattern between proteins could be associated with a similar reactivity (Repič2014). Contrarily, the electrostatic organization of hIDO2 compared to hIDO1 is modified and it might be possible that this further influences the enzymatic reactivity (Schwartz2023)

Table 1: pKa of key residues in hIDO1 and hIDO2 calculated by the PropKa server. (Li2005)

hIDO1			hIDO2	
Residues	pKa in intermediate position (PDB code: 7p0r)	pKa in pre-reactive position (PDB code: 7nge)	Residues	pKa in MD pos1 structure after 300ns
Y126	16.49	16.30	H130	-1.26
C129	11.52	11.81	L133	/
R231	10.21	12.70	R235	13.23

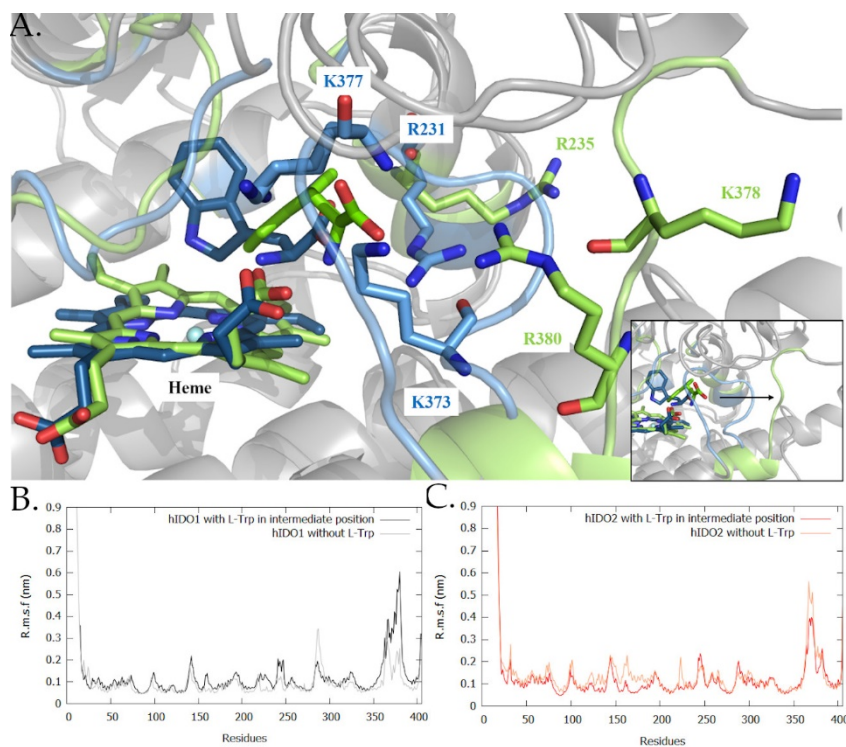| K373	9.50	7.63	A375	/
E375	4.53	4.97	K378	10.22
K377	10.00	9.06	R380	10.81

Figure 10: Structural comparison of hIDO1 and hIDO2 proteins with L-Trp in their active site. A. Superimposition of the hIDO1/L-Trp in pre-reactive position structure (PDB code: 7nge, in blue) and hIDO2/L-Trp in intermediate position (after 300 ns of MD simulation, in green). Residues at 4 Å of the ligands are highlighted in the corresponding colors. Residues with different electrostatic pre-organization are shown with stick. Lower right corner: different pre-organization of the residues of the dynamic loops JK and JK'. The arrow points to difference in term of position for the JK and the JK'-loops. B. R.m.s.f. profiles of hIDO1 in presence or in absence of L-Trp with the JK-loop in the intermediate position. C. R.m.s.f. profiles of hIDO2 in presence or in absence of L-Trp in the intermediate position.

In addition to this, the nature of the amino acid residues changes between the active site of the two proteins. For the JK-loop of hIDO1 and the JK'-loop of hIDO2, the replacement of K373 and E375 in

hIDO1 by A375 and K378 in hIDO2 leads to a change in polarity and pKa values of the loop (**Table 1**). In addition to this effect of the JK'-loop, as mentioned by Roehrig *et al*. (Roehrig2016), four amino acids are not conserved in the catalytic pocket (Y126, C129, F164, and S167 of hIDO1 are replaced by H130, L133, I168, and T171 for hIDO2, respectively), inducing a 15% increase in the pocket size. While long-range electrostatic interactions might be considered to be less important for determining pKa values (Sham1997), the difference in the amino acid composition of the hIDO1 and hIDO2 active sites has a large effect on their residue pKa values. Indeed, the calculated pKa values show that the basicity of C129 of hIDO1 tends to increase the deeper the substrate is positioned inside the active site, i.e., it rises from 11.52 to 11.81 (**Table 1**). The analog in hIDO2, i.e., L133, has no acid/base properties. Conversely, H130 in hIDO2 has a much more acidic pKa (-1.26) than Y126 in hIDO1 (16.49). Those two pKa values predicted by PropKa are extreme. Nevertheless, they suggest a clear discrepancy in the electrostatic environment of the active site while the literature mentions that identical pre-organization patterns between proteins could be associated with a similar reactivity (Repič2014). To summarize, the poor activity of hIDO2 might be linked to an unfavorable initial positioning of L-Trp in the active site compared to hIDO1, a different electrostatic pre-organization between the two proteins and the absence of plasticity of the JK'-loop.

Conclusions

Although hIDO2 shows an increasing interest as a therapeutic target, it is poorly characterized in the literature, with a lack of structural information. In this paper, the protein was characterized through a multidisciplinary approach mixing homology modeling, MD simulations, and molecular docking calculations. All the results converge towards a model for hIDO2 which presents flexibility at the F' helix and at the JK' loop. These parts are strongly affected by the absence of the cofactor, mutations, and/or deletions. It results in a potential lability of the heme cofactor in the holo form and an inability to bind the cofactor in the apo form. In several simulations, it was shown that this effect was favored by the conformational change of the G' and I' helices. Following important induced fit rearrangements, the polymorphs (R235W and Y346X) observed in the Caucasian populations also show a loss of cofactor coordination, which might be a factor among those at the origin of their poor activity. The binding of

the substrate to the enzyme has also been studied. Through molecular docking and MD simulations, it is shown that the substrate does not easily position itself in a pre-reactive state within the active site of hIDO2. This supports the fact that the affinity of L-Trp for the enzyme is low. The substrate mainly adopts an misoriented position in the active site, even if the active site pocket is open. In this case, the JK'-loop is relatively stable and is characterized by an intermediate conformation for the C-terminal part. This stabilization does not lead to the closing of the active site and does not push L-Trp into pocket A. In addition, changes of residue pKa values in comparison to hIDO1 affect the electrostatic pre-organization of the enzyme.

To conclude, as the cofactor is an essential partner to the reaction, increasing its lability results in a decrease of the enzymatic activity. Moreover, the positioning of L-Trp in the active site remains mostly a non-ideal one in hIDO2 and can be a reason for the lack of affinity of the substrate, a decrease of the JK'-loop plasticity, and a change in term of electrostatic pre-organization in comparison to hIDO1. Taken together, these effects are consistent with the poor activity of the protein. The present model thus helps to understand the hIDO2 system until experimental structural data are obtained. A step beyond conventional MD modeling of enzymes is to consider Quantum Mechanical approaches combined with good sampling methods to investigate enzyme reaction mechanisms. Thus, methods relevant to the so-called multiscale QM/MM approach, are often used to model protein systems. Recent reviews or perspective works in the field can be found in, e.g., (Olsson2017, Bauer2018, Giudetti2022, Tzeliou2022, Vennelakanti2022). In their paper, Warshel and Bora (Warshel2016) suggest that the Empirical Valence Bond (EVB) is an effective way of exploring enzymatic reactivity. In particular, the Q6 software is designed to perform MD as well as free energy calculations of enzymatic reactions (Bauer2018). It allows EVB/MM calculations which is expected to provide extensive conformational sampling and sufficient chemical information to describe chemical processes (Duarte2015). Pre-organized substrate arrangements in hIDO1 and hIDO2 studied in the present work can be considered as starting points for further QM/MM modeling of the reaction mechanism.

Conflict of Interest Statement

The authors declare that they have no conflicts of interest.

Acknowledgments

References

Abraham, M. J., Murtola, T., Schulz, R., Páll, S., Smith, J. C., Hess, B., & Lindahl, E. (2015). GROMACS: High performance molecular simulations through multi-level parallelism from laptops to supercomputers. *SoftwareX*, *1*, 19-25.

Austin, C. J., & Rendina, L. M. (2015). Targeting key dioxygenases in tryptophan–kynurenine metabolism for immunomodulation and cancer chemotherapy. *Drug discovery today*, *20*(5), 609-617.

Ball, H. J., Sanchez-Perez, A., Weiser, S., Austin, C. J., Astelbauer, F., Miu, J., McQuillan, J. A., Stocker, R., Jermiin, L. S. & Hunt, N. H. (2007). Characterization of an indoleamine 2, 3-dioxygenase-like protein found in humans and mice. *Gene*, *396*(1), 203-213.

Ball, H. J., Yuasa, H. J., Austin, C. J., Weiser, S., & Hunt, N. H. (2009). Indoleamine 2, 3-dioxygenase-2; a new enzyme in the kynurenine pathway. *The international journal of biochemistry & cell biology*, *41*(3), 467-471.

Bauer, P., Barrozo, A., Purg, M., Amrein, B. A., Esguerra, M., Wilson, P. B., Major, D. M., Åqvist, J., & Kamerlin, S. C. L. (2018). Q6: A comprehensive toolkit for empirical valence bond and related free energy calculations. *SoftwareX*, *7*, 388-395.

Chilosi, M., Doglioni, C., Ravaglia, C., Martignoni, G., Salvagno, G. L., Pizzolo, G., Bronte, G. & Poletti, V. (2022). Unbalanced IDO1/IDO2 Endothelial Expression and Skewed Keynurenine Pathway in the Pathogenesis of COVID-19 and Post-COVID-19 Pneumonia. *Biomedicines*, *10*(1332), 1-24.

Corpet, F. (1988). Multiple sequence alignment with hierarchical clustering. *Nucleic acids research*, *16*(22), 10881-10890.

Dolšak, A., Gobec, S., & Sova, M. (2021). Indoleamine and tryptophan 2, 3-dioxygenases as important future therapeutic targets. *Pharmacology & Therapeutics*, *221*, 1-23.

Duarte, F., Amrein, B. A., Blaha-Nelson, D., & Kamerlin, S. C. L. (2015) Recent advances in QM/MM free energy calculations using reference potentials. *Biochimica et Biophysica Acta, 1850*(5), 954–965

Fallarino, F., Grohmann, U., & Puccetti, P. (2012). Indoleamine 2, 3-dioxygenase: from catalyst to signaling function. *European journal of immunology*, *42*(8), 1932-1937.

Fatokun, A. A., Hunt, N. H., & Ball, H. J. (2013). Indoleamine 2, 3-dioxygenase 2 (IDO2) and the kynurenine pathway: characteristics and potential roles in health and disease. *Amino acids*, *45*, 1319-1329.

Giudetti, G., Polyakov, I., Grigorenko, B. L., Faraji, S., Nemukhin, A. V., & Krylov, A. I. (2022). How Reproducible Are QM/MM Simulations? Lessons from Computational Studies of the Covalent Inhibition of the SARS-CoV-2 Main Protease by Carmofur. *Journal of Chemical Theory and Computation*, *18*(8), 5056-5067.

Greenwood, J. R., Calkins, D., Sullivan, A. P., & Shelley, J. C. (2010). Towards the comprehensive, rapid, and accurate prediction of the favorable tautomeric states of drug-like molecules in aqueous solution. *Journal of computer-aided molecular design*, *24*(6-7), 591-604.

Guex, N., Peitsch, M. C., & Schwede, T. (2009). Automated comparative protein structure modeling with SWISS-MODEL and Swiss-PdbViewer: A historical perspective. *Electrophoresis*, *30*(S1), S162-S173.

Guo, L., Schurink, B., Roos, E., Nossent, E. J., Duitman, J. W., Vlaar, A. P., van der Valk, P., Vaz, F. M., Yeh, S-Y., Geeraerts, Z., Dijkhuis, A., van Vulght, L., Bugiani, M., & Lutter, R. (2022). Indoleamine 2, 3-dioxygenase (IDO)-1 and IDO-2 activity and severe course of COVID-19. *The Journal of pathology*, *256*(3), 256-261.

Harder, E., Damm, W., Maple, J., Wu, C., Reboul, M., Xiang, J. Y., Wang, L., Lupyan, D., Dahlgren, M. K., Knight, J. L., Kaus, J. W., Cerutti, D. S., Krilov, G., Jorgensen, W. L., Abel, R. & Friesner, R. A. (2016). OPLS3: a force field providing broad coverage of drug-like small molecules and proteins. *Journal of chemical theory and computation*, *12*(1), 281-296.

He, X., He, G., Chu, Z., Wu, H., Wang, J., Ge, Y., Shen, H., Zhang, S., Shan, J. Peng, K. Wei, Z., Zou, Y. Xu, Y., & Zhu, Q. (2021). Discovery of the first potent IDO1/IDO2 dual inhibitors: a promising strategy for cancer immunotherapy. *Journal of Medicinal Chemistry*, *64*(24), 17950-17968.

Jacobson, M. P., Friesner, R. A., Xiang, Z., & Honig, B. (2002). On the role of the crystal environment in determining protein side-chain conformations. *Journal of molecular biology*, *320*(3), 597-608.

Jacobson, M. P., Pincus, D. L., Rapp, C. S., Day, T. J., Honig, B., Shaw, D. E., & Friesner, R. A. (2004). A hierarchical approach to all-atom protein loop prediction. *Proteins: Structure, Function, and Bioinformatics*, *55*(2), 351-367.

Jumper, J., Evans, R., Pritzel, A., Green, T., Figurnov, M., Ronneberger, O., Tunyasuvunakool, K., Bates, R., Žídek, A., Potapenko, A., Bridgland, A., Meyer, C., Kohl, S. A. A., Ballard, A. J., Cowie, A., Romera-Paredes, B., Nikolov, S., Jain, R., Adler, J., Back, T., Petersen, S., Reiman, D., Clancy, E., Zielinski, M., Steinegger, M., Pacholska, M., Berghammer, T., Bodenstein, S., Silver, D., Vinyals, O., Senior, A. W., Kavukcuoglu, K., Kohli P., & Hassabis, D. (2021). Highly accurate protein structure prediction with AlphaFold. *Nature*, *596*(7873), 583-589.

Lee, Y. K., Lee, H. B., Shin, D. M., Kang, M. J., Yi, E. C., Noh, S., Lee, J., Lee, C., Min, C-K, & Choi, E. Y. (2014). Heme-binding-mediated negative regulation of the tryptophan metabolic enzyme indoleamine 2, 3-dioxygenase 1 (IDO1) by IDO2. *Experimental & molecular medicine*, *46*(11), 1-11.

Li, H., Robertson, A. D., & Jensen, J. H. (2005). Very fast empirical prediction and rationalization of protein pKa values. *Proteins: Structure, Function, and Bioinformatics*, *61*(4), 704-721.

Li, J., Abel, R., Zhu, K., Cao, Y., Zhao, S., & Friesner, R. A. (2011). The VSGB 2.0 model: a next generation energy model for high resolution protein structure modeling. *Proteins: Structure, Function, and Bioinformatics*, *79*(10), 2794-2812.

Li, P., Xu, W., Liu, F., Zhu, H., Zhang, L., Ding, Z., Liang, H., & Song, J. (2021). The emerging roles of IDO2 in cancer and its potential as a therapeutic target. *Biomedicine & Pharmacotherapy*, *137*, 1-6.

Long, G. V., Dummer, R., Hamid, O., Gajewski, T. F., Caglevic, C., Dalle, S., Arance, A., Carlino, M. S., Grob, J.-J., Kim, T. M., Demidov, L., Robert, C., Larkin, J., Anderson, J. R., Maleski, J., Jones, M., Diede, S. J., & Mitchell, T. C. (2019). Epacadostat plus pembrolizumab versus placebo plus pembrolizumab in patients with unresectable or metastatic melanoma (ECHO-301/KEYNOTE-252): a phase 3, randomised, double-blind study. *The Lancet Oncology*, *20*(8), 1083-1097.

Löb, S., Königsrainer, A., Zieker, D., Brücher, B. L., Rammensee, H. G., Opelz, G., & Terness, P. (2009). IDO1 and IDO2 are expressed in human tumors: levo-but not dextro-1-methyl tryptophan inhibits tryptophan catabolism. *Cancer immunology, immunotherapy*, *58*, 153-157.

MacKerell Jr, A. D., Banavali, N., & Foloppe, N. (2000). Development and current status of the CHARMM force field for nucleic acids. *Biopolymers: original Research on biomolecules*, *56*(4), 257-265.

Madhavi Sastry, G., Adzhigirey, M., Day, T., Annabhimoju, R., & Sherman, W. (2013). Protein and ligand preparation: parameters, protocols, and influence on virtual screening enrichments. *Journal of computer-aided molecular design*, *27*, 221-234.

Mandarano, M., Bellezza, G., Belladonna, M. L., Vannucci, J., Gili, A., Ferri, I., Lupi, C., Ludovini, V., Falabella, G., Metro, G., Mondanelli, G., Chiari, R., Cagini, L., Stracci, F., Roila, F., Puma, F., Volpi, C., & Sidoni, A. (2020). Indoleamine 2, 3-dioxygenase 2 immunohistochemical expression in resected human non-small cell lung cancer: a potential new prognostic tool. *Frontiers in Immunology*, *11*, 1-10.

McGeagh, J. D., Ranaghan, K. E., & Mulholland, A. J. (2011). Protein dynamics and enzyme catalysis: insights from simulations. *Biochimica et Biophysica Acta (BBA)-Proteins and Proteomics*, *1814*(8), 1077-1092.

Meininger, D., Zalameda, L., Liu, Y., Stepan, L. P., Borges, L., McCarter, J. D., & Sutherland, C. L. (2011). Purification and kinetic characterization of human indoleamine 2, 3-dioxygenases 1 and 2 (IDO1 and IDO2) and discovery of selective IDO1 inhibitors. *Biochimica et biophysica acta (BBA)-proteins and Proteomics*, *1814*(12), 1947-1954.

Merlo, L. M., DuHadaway, J. B., Montgomery, J. D., Peng, W. D., Murray, P. J., Prendergast, G. C., Caton, A. J., Muller, A.J., & Mandik-Nayak, L. (2020). Differential roles of IDO1 and IDO2 in T and B cell inflammatory immune responses. *Frontiers in Immunology*, *11*, 1-16.

Merlo, L. M., Bowers, J., Stefanoni, T., Gordon, G. V., Getts, R., & Mandik-Nayak, L. (2021). The immunomodulating enzyme indoleamine 2, 3-dioxygenase 2 (IDO2) as a target for therapy in autoimmune disease. *The Journal of Immunology*, *206*(1_Supplement), 66-01.

Mirgaux, M., Leherte, L., & Wouters, J. (2020). Influence of the presence of the heme cofactor on the JK-loop structure in indoleamine 2, 3-dioxygenase 1. *Acta Crystallographica Section D: Structural Biology*, *76*(12), 1211-1221.

Mirgaux, M., Leherte, L., & Wouters, J. (2021). Temporary Intermediates of L-Trp Along the Reaction Pathway of Human Indoleamine 2, 3-Dioxygenase 1 and Identification of an Exo Site. *International Journal of Tryptophan Research*, *14*, 1-11.

M. Mirgaux. (2022) *Plasticity of human indoleamine-2,3-dioxygenases 1 and 2 through a structural approach combining crystallography and Molecular Dynamics studies* [PhD thesis, University of Namur].

Mondanelli, G., Mandarano, M., Belladonna, M. L., Suvieri, C., Pelliccia, C., Bellezza, G., Sidoni, A., Carvalho, A., Grohmann, U. & Volpi, C. (2021). Current challenges for IDO2 as target in cancer immunotherapy. *Frontiers in Immunology*, *12*, 1-7.

Pantouris, G., Serys, M., Yuasa, H. J., Ball, H. J., & Mowat, C. G. (2014). Human indoleamine 2, 3-dioxygenase-2 has substrate specificity and inhibition characteristics distinct from those of indoleamine 2, 3-dioxygenase-1. *Amino acids*, *46*, 2155-2163.

Olsson, M. A., & Ryde, U. (2017). Comparison of QM/MM methods to obtain ligand-binding free energies. *Journal of chemical theory and computation*, *13*(5), 2245-2253.

Opitz, C. A., Somarribas Patterson, L. F., Mohapatra, S. R., Dewi, D. L., Sadik, A., Platten, M., & Trump, S. (2020). The therapeutic potential of targeting tryptophan catabolism in cancer. *British journal of cancer*, *122*(1), 30-44.

Repič, M., Purg, M., Vianello, R., & Mavri, J. (2014). Examining electrostatic preorganization in monoamine oxidases A and B by structural comparison and pKa calculations. *The Journal of Physical Chemistry B*, *118*(16), 4326-4332.

Roehrig, U. F., Majjigapu, S. R., Caldelari, D., Dilek, N., Reichenbach, P., Ascencao, K., Irving, M., Coukos, G., Vogel, P., Zoete, V., & Michielin, O. (2016). 1, 2, 3-Triazoles as inhibitors of indoleamine 2, 3-dioxygenase 2 (IDO2). *Bioorganic & medicinal chemistry letters*, *26*(17), 4330-4333.

Schrödinger, LLC. The PyMOL molecular graphics system. Version 1.7.4.4, November 2015.

Schwartz, S. D. (2023). Protein dynamics and enzymatic catalysis. *The Journal of Physical Chemistry B*, *127*(12), 2649-2660.

Sham, Y. Y., Chu, Z. T., & Warshel, A. (1997). Consistent calculations of pKa's of ionizable residues in proteins: semi-microscopic and microscopic approaches. *The Journal of Physical Chemistry B*, *101*(22), 4458-4472.

Shelley, J. C., Cholleti, A., Frye, L. L., Greenwood, J. R., Timlin, M. R., & Uchimaya, M. (2007). Epik: a software program for pK a prediction and protonation state generation for drug-like molecules. *Journal of computer-aided molecular design*, *21*, 681-691.

Studer, G., Rempfer, C., Waterhouse, A. M., Gumienny, R., Haas, J., & Schwede, T. (2020). QMEANDisCo—distance constraints applied on model quality estimation. *Bioinformatics*, *36*(6), 1765-1771.

The UniProt Consortium. (2021) UniProt: the universal protein knowledgebase in 2021. *Nucleic acids research*, 49(D1), D480-D489.

Tzeliou, C. E., Mermigki, M. A., & Tzeli, D. (2022). Review on the QM/MM methodologies and their application to metalloproteins. *Molecules*, *27*(9), 2660.

Uyttenhove, C., Pilotte, L., Théate, I., Stroobant, V., Colau, D., Parmentier, N., Boon, T., & Van den Eynde, B. J. (2003). Evidence for a tumoral immune resistance mechanism based on tryptophan degradation by indoleamine 2, 3-dioxygenase. *Nature medicine*, *9*(10), 1269-1274.

Varadi, M., Anyango, S., Deshpande, M., Nair, S., Natassia, C., Yordanova, G., Yuan, D., Stroe, O., Wood, G., Laydon, A., Žídek, A., Green, T., Tunyasuvunakool, K., Petersen, S., Jumper, J., Clancy, E., Green, R., Vora, E., Lutfi, M., Figurnov, M., Cowie, A., Hobbs, N., Kohli, P., Kleywegt, G., Birney, E., Hassabis, D., & Velankar, S. (2022). AlphaFold Protein Structure Database: massively expanding the structural coverage of protein-sequence space with high-accuracy models. *Nucleic acids research*, *50*(D1), D439-D444.

Vennelakanti, V., Nazemi, A., Mehmood, R., Steeves, A. H., & Kulik, H. J. (2022). Harder, better, faster, stronger: Large-scale QM and QM/MM for predictive modeling in enzymes and proteins. *Current opinion in structural biology*, *72*, 9-17.

Warshel, A., & Bora, R. P. (2016). Perspective: Defining and quantifying the role of dynamics in enzyme catalysis. *The Journal of chemical physics*, *144*(18), 180901.

Zoete, V., Cuendet, M. A., Grosdidier, A., & Michielin, O. (2011). SwissParam: a fast force field generation tool for small organic molecules. *Journal of computational chemistry*, *32*(11), 2359-2368.

Human indolenamine-2,3-dioxygenase 2 cofactor lability and low substrate affinity explained by homology modeling, Molecular Dynamics and Molecular Docking – Supplementary Material

Manon Mirgaux[a], Laurence Leherte[a], Johan Wouters[a]

a Namur Institute of Structured Matter (NISM), Namur Research Institute for Life, Science (NARILIS), Department of Chemistry, Laboratoire de Chimie Biologique, Structurale (CBS), University of Namur (UNamur), 61 Rue de Bruxelles, 5000, Namur, Belgium

Correspondance email: Manon Mirgaux, +32 81 72 45 69, manon.mirgaux@unamur.be, Johan Wouters, +32 81 72 45 50, johan.wouters@unamur.be
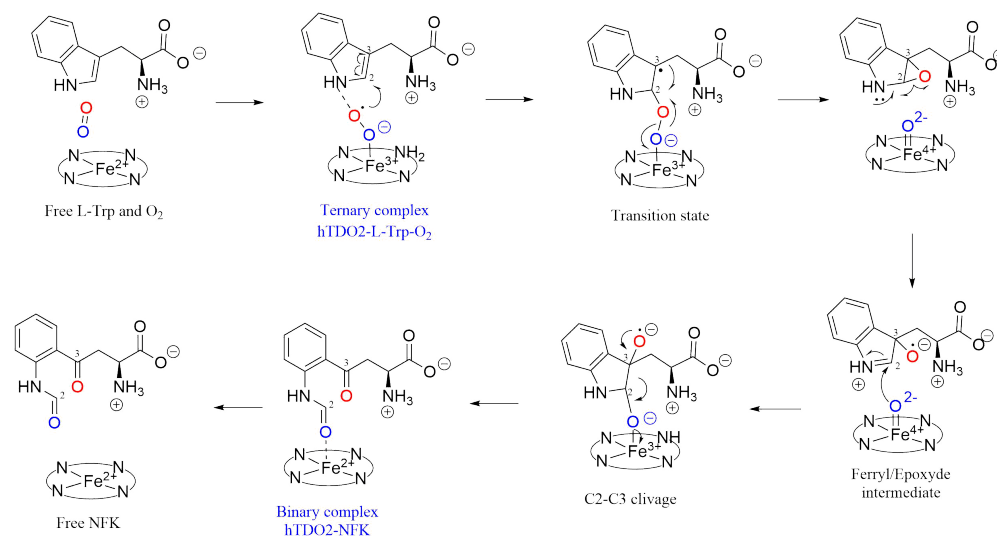
Figure S1: Mechanism of hIDO1 according to the hypothesis developed by Basran *et al.*. (Basran2016, Efimov2011).

In hIDO1, the heme cofactor activates the dioxygen using a radical addition. Using this activated molecule of O2, hIDO1 converts L-Trp to NFK by oxidative cleavage of the C2-C3 double bond of the indole moiety. The radical addition of O_2 breaks the double bond of the indole to form a single bond and a radical on the C3 of L-Trp. The resulting intermediate is a peroxide ion which the bond between

the two oxygens will be broken to form an epoxide intermediate. Then, the second oxygen allows the opening of the epoxide, followed by the breaking of the bond between C2 and C3 and the formation of two carbonyls to form NFK. The hIDO1 enzyme is not very specific to its substrate which leads to the possible catalysis of several indoleamine derivatives (L-Trp, D-Trp, serotonin, 5-hydroxy-L-Trp, etc.). For L-Trp, the current data shows an affinity of the protein for the substrate in the micro-molar range (Michaelis constant (Km) of 40 μM). The enzymatic activity is also particular since an inhibition by the substrate is observed at high concentration. (Röhrig2021) To perform the catalytic reaction, the heme must be in ferrous form at the beginning of the reaction cycle. Scientific evidence suggests that, in vivo, this is achieved with the help of cytochrome b5 and cytochrome P450 reductase with NADPH. (Maghzal 2008) Dioxygen binding occurs before L-Trp binding in hIDO1. In hIDO2, no information is available. The mechanism of hIDO2 is still undetailed in the literature. It seems that the protein is less prone to auto-oxidation and that it can perform several catalytic cycles before being in the auto-oxidation phase. (Yuasa2021)
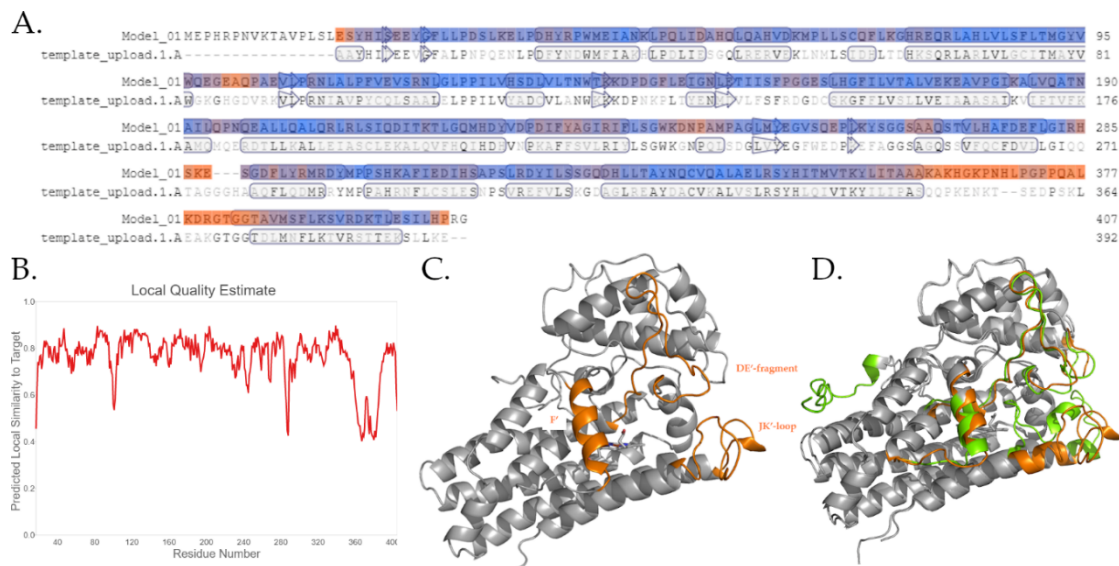

Figure S2: Homology modelling of the structure of hIDO2 achieved with the SwissModel software. A. Local model quality evaluation. Low quality is represented in orange while high quality is in blue. B. Local Quality Estimation C. HIDO2 homology model. D. Superimposition of the SwissModel and the AlphaFold models. (Jumper2021, Varadi2022) The divergent areas in the tertiary structure are highlighted, respectively, in green for AlphaFold and in orange for the SwissModel.
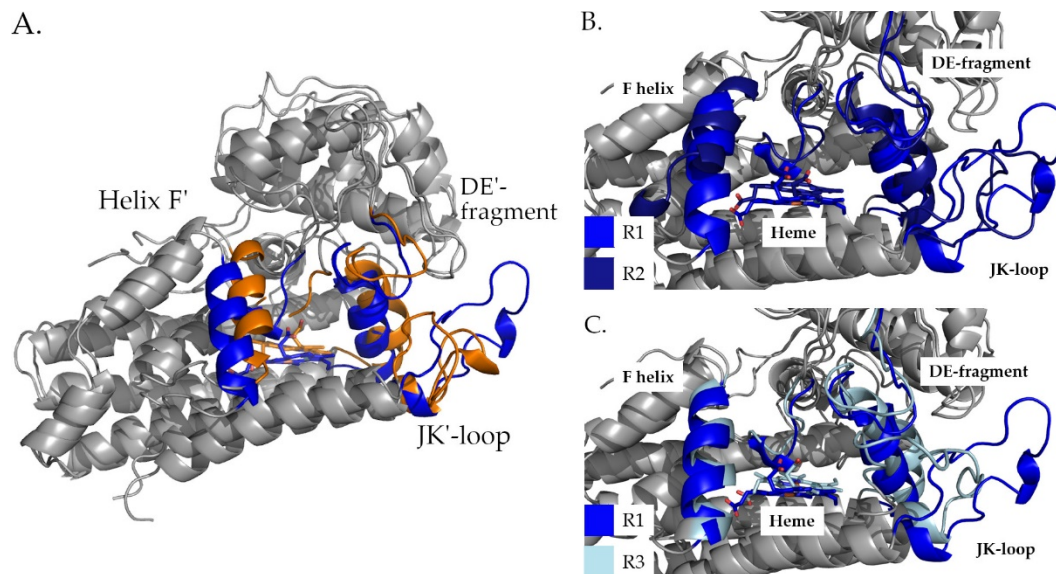
Figure S3: Structural differences between the SwissModel homology model (in orange) and the MD replicates after 300 ns of MD simulations at 310 K and 1 bar (in different shades of blue: R1 = medium blue, R2 = dark blue, and R3 = light blue) for holo hIDO2. A. Differences highlighted between the homology model and R1. B. Structural differences (highlighted in colors) between the rep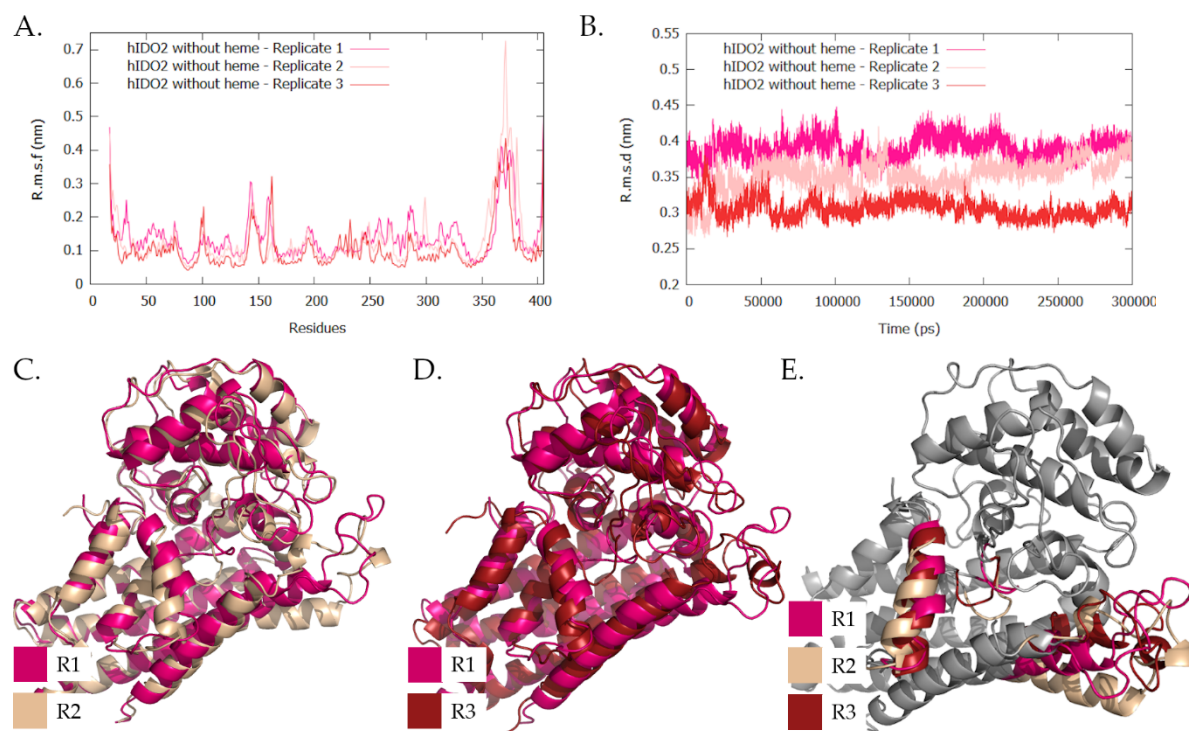licates R1 and R2 (mainly localized at the helix F' and heme binding site). C. Structural differences (highlighted in colors) between the replicates R1 and R3 (mainly localized at the JK'- and DE'-fragment).

Figure S4: Structural differences (highlighted in colors) between the MD replicates of apo hIDO2 after 300 ns at 310 K and 1 bar (in different shades of red: R1 = dark pink, R2 = wheat, and R3 = red). A. R.m.s.f. profiles of hIDO2. B. R.m.s.d. profiles of each replicate obtained using the corresponding starting structure as the reference one. C. Comparison of the folding between R1 and R2. D. Comparison of the folding between R1 and R3. E. Comparison of the folding for the three replicates
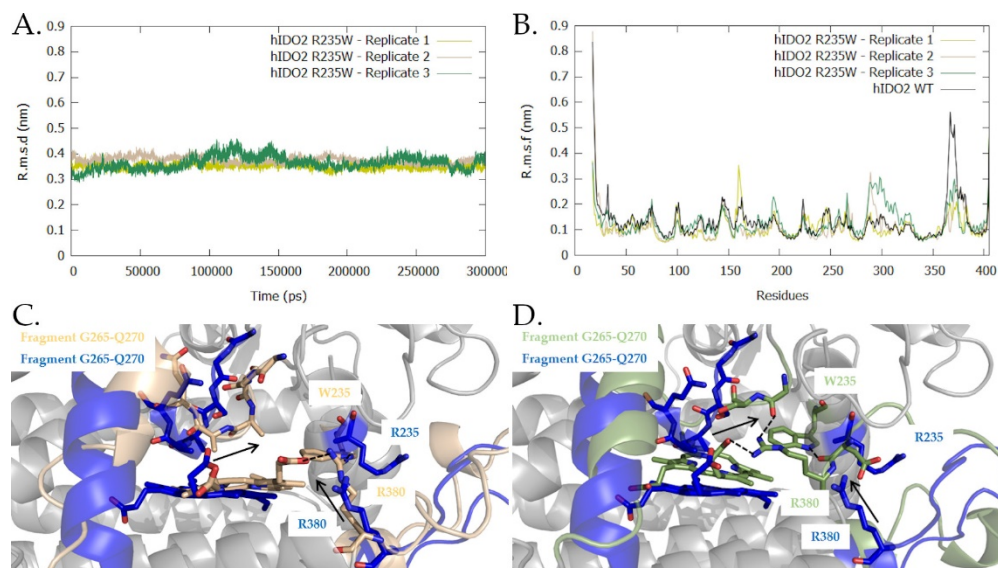
Figure S5: Conformation of the mutated R235W hIDO2 protein after a 300 ns MD simulation, at 310 K and 1 bar. A. R.m.s.d. of the protein using the corresponding starting structure at the reference one. B. R.m.s.f. profiles on the protein for the three replicates and comparison with the WT protein. C. Induced-fit due to the R235W mutation on the JK'-loop residues for R2. D. Induced-fit due to the R235W mutation on the JK'-loop residues for R3.
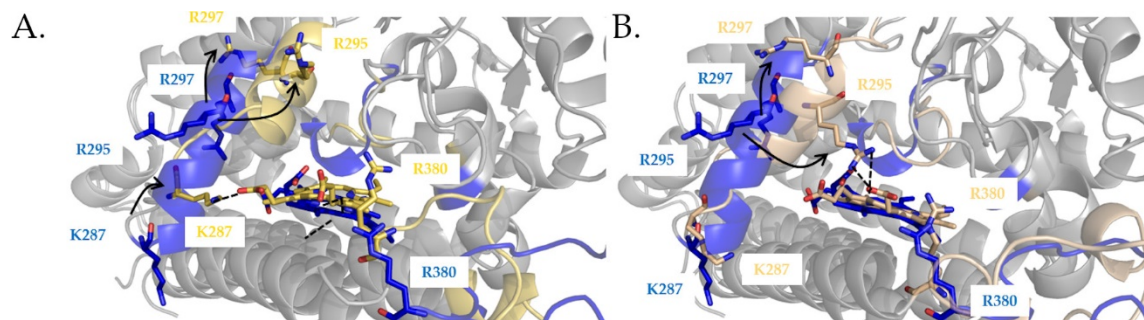
Figure S6: Induced-fit caused by the R235W mutation in the F' helix of hIDO2. Conformation of the protein after a 300 ns MD simulation, at 310 K and 1 bar. A. For R1. B. For R2.
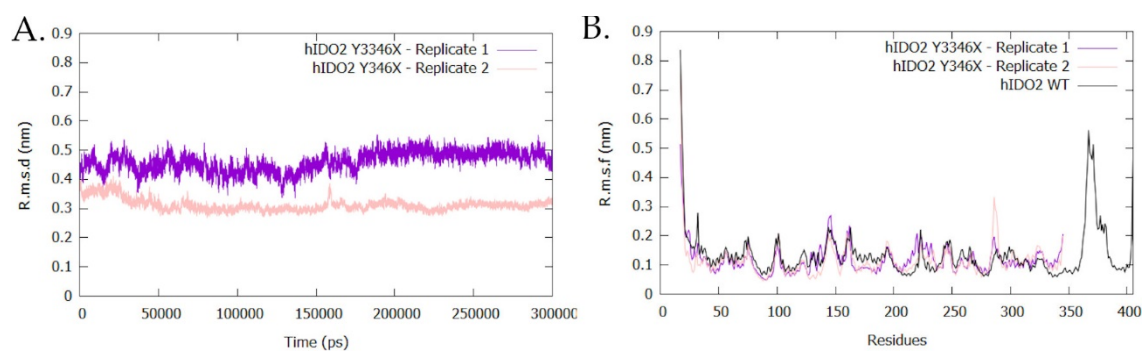

Figure S7: Conformation of the Y346X hIDO2 protein after a 300 ns of MD simulation, at 310 K and 1 bar. A. R.m.s.d. profiles calculated with respect to the corresponding starting structure. B. R.m.s.f. profiles of the protein residues for the replicates and the WT protein.
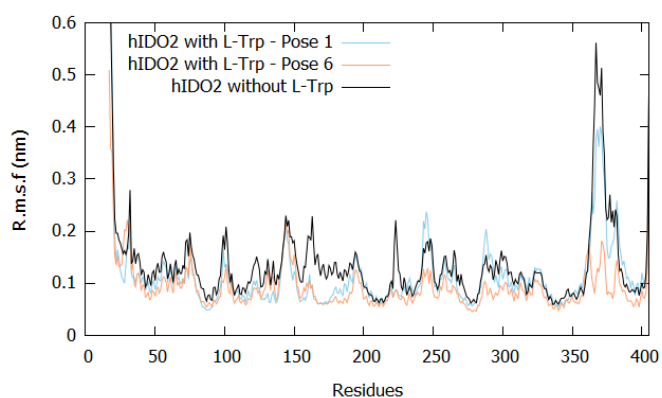

Figure S8: R.m.s.f. profiles of the hIDO2 protein residues for L-Trp bound simulations with pos1 and pos6.
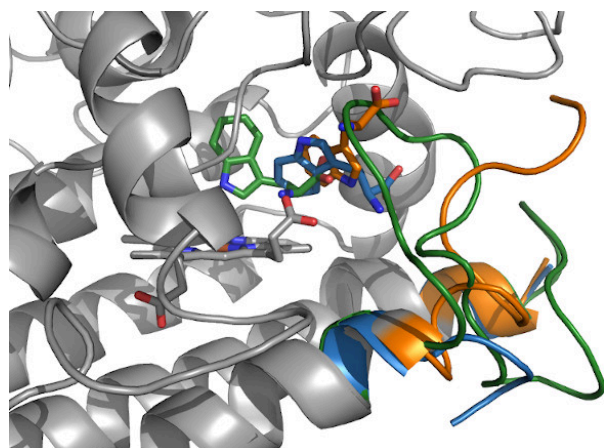
Figure S9: Crystal structures of hIDO1 with L-Trp was observed in three distinct positions. L-Trp occupies an intermediate position (blue and orange, respectively PDB code: 7p0n and 7p0r) while the third one presents L-Trp in a pre-reactive position (green, PDB code: 7nge).
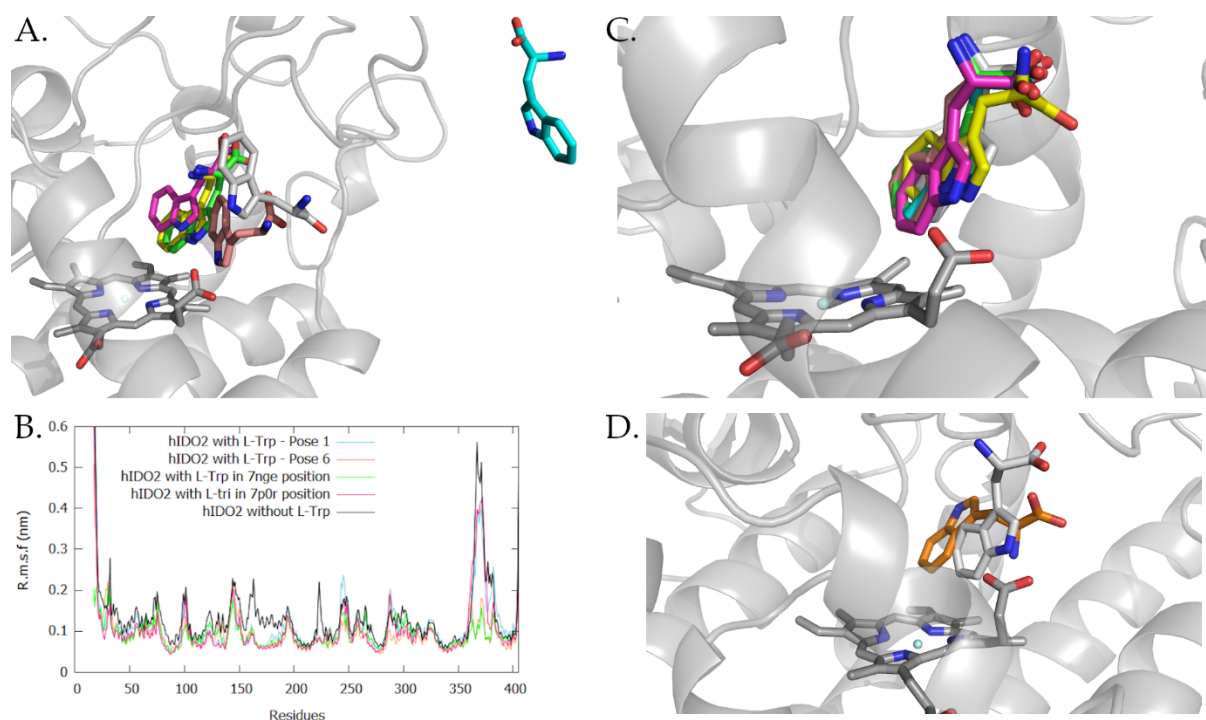

Figure S10: A. Snapshots of the 300 ns MD trajectories of the L-Trp bound to hIDO2 at 1, 10, 20, 30, 40, and 50 ns, at 310 K and 1 bar. The starting L-Trp position is based on the position observed in hIDO1-closed (PDB: 7nge). L-Trp leaves the active site during the simulation. B. R.m.s.f. profiles of the protein residues for the different simulations. C. Snapshots of the 300 ns MD trajectories of the L-Trp bound to hIDO2 at 50, 100, 150, 200, 250, and 300 ns, at 310 K and 1 bar. The starting L-Trp position is based on the position observed in hIDO1- intermediate (PDB: 7p0r) and is used as the starting

MD ligand position. L-Trp remains at a misoriented position in the active site during simulation. D. Comparison of the position of L-Trp after 300 ns of simulation in case of a starting pos1 position (grey) and a starting hIDO1-intermediate position (PDB: 7p0r, orange).

Complementary computational experiments

Influence of M350 on heme lability

The helix I' sequence alignment of hIDO2 with hIDO1 shows two major changes in the H347 environment for hIDO2 (**Figure S10**, A.). In the case of the hIDO2, residues 349 and 350 are a threonine and a methionine instead of a glutamine and an isoleucine in hIDO1. M350 is of particular interest because it is oriented below the heme cofactor in the WT protein, which is not the case for T349 (**Figure S6**, B.). Triplicate MD simulations were performed on hIDO2 as an M350I mutant. The results obtained are presented in **Table S1** and **Figure S10**. The three replicates are consistent with each other in terms of global folding, average fluctuation, and convergence.

Table S1: Distances (in Å) between H347 (NE) and the central iron of the heme cofactor. The analysis was performed on the 300 ns of MD simulations at 310 K and 1 bar, for each replicate.

Residue 350	R1	R2	R3
Methionine	5.8 +/- 1.5	6.4 +/- 1.4	6.9 +/- 0.5
Isoleucine	9.0 +/- 0.7	5.5 +/- 1.4	9.2 +/- 0.8

In the hIDO2 WT simulation, M350 is close to H347 (**Table S1**). One of the working hypotheses is that this vicinity favors the motion of H347 and causes a loss of coordination between H347 and the cofactor. This loss of coordination can be responsible for the displacement of the heme in the active site. However, it is found with the M350I simulations that such a hypothesis is not valid. Indeed, the protein motion is identical with or without mutation (**Figure S10**, C.), and is particularly weak for residues H347-M350. The MD results show that I350 is placed in a similar way to M350 in hIDO2 (**Figure S10**, D.). Also, the mutation has no effect on the JK'-loop, which remains in an open configuration, with high flexibility according to the replicates. In contrast to what would have been imagined, the mutation applied to mimic the hIDO1 sequence unfavors the binding of the heme. While H347 and I350 are oriented in the same way in the replicates, the magnitude of the heme motion varies into the different replicates, inducing variable distances between H347 and the iron atom. The H347(NE)-iron distance

values increase drastically in R1 and R3 (**Table 1**). It is concluded that the M350 does not unfavor the binding of the heme to hIDO2. Additionally, M350 helps to keep the heme inside the active site. Consequently, the loss of coordination between the heme and H347 and the cofactor displacement is caused by the conformational change of the F' helix and the G265-Q270 fragment.
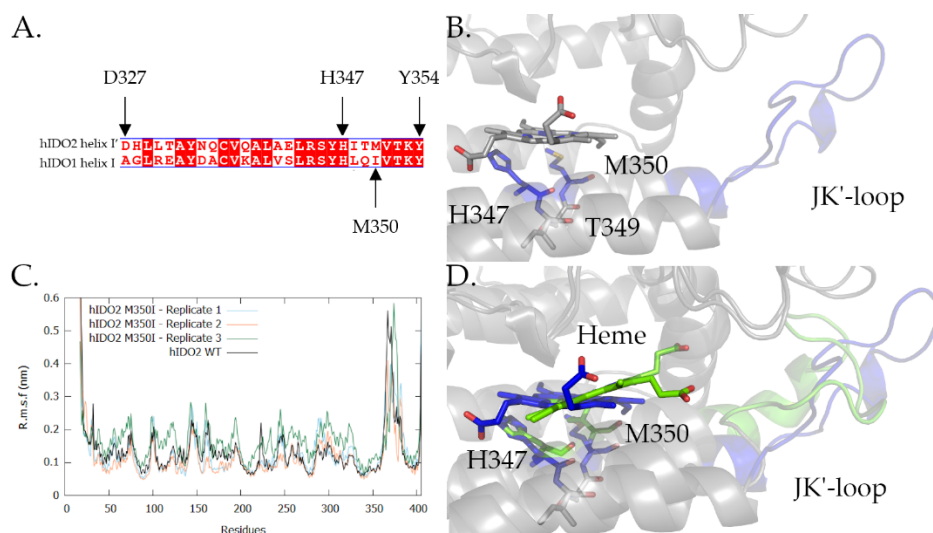

Figure S10: Effect of the M350I mutation on the position of the heme in the active site. A. Sequence alignment of helix I in hIDO1 and I' in hIDO2. B. Active site of WT hIDO2. C. R.m.s.f profiles of hIDO2 with or without the M350I mutation. D. Relative positioning of H347, I350, and the cofactor with the mutant protein (R1) compared to the WT protein.

References

Basran, J., Booth, E. S., Lee, M., Handa, S., & Raven, E. L. (2016). Analysis of reaction intermediates in tryptophan 2, 3-dioxygenase: a comparison with indoleamine 2, 3 dioxygenase. *Biochemistry*, *55*(49), 6743-6750.

Efimov, I., Basran, J., Thackray, S. J., Handa, S., Mowat, C. G., & Raven, E. L. (2011). Structure and reaction mechanism in the heme dioxygenases. *Biochemistry*, *50*(14), 2717-2724.

Maghzal, G. J., Thomas, S. R., Hunt, N. H., & Stocker, R. (2008). Cytochrome b5, not superoxide anion radical, is a major reductant of indoleamine 2, 3-dioxygenase in human cells. *Journal of Biological Chemistry*, *283*(18), 12014-12025.

Röhrig, U. F., Michielin, O., & Zoete, V. (2021). Structure and plasticity of indoleamine 2, 3-dioxygenase 1 (IDO1). *Journal of Medicinal Chemistry*, *64*(24), 17690-17705.

Yuasa, H. J., & Stocker, R. (2021). Methylene blue and ascorbate interfere with the accurate determination of the kinetic properties of IDO2. *The FEBS Journal*, *288*(16), 4892-4904.